

# **3D Visualization of Hill-Sachs Lesions with Articulation**

**Jordan Terrence Crawford**

**A Thesis**

**in**

**The Department**

**of**

**Computer Science and Software Engineering**

**Presented in Partial Fulfillment of the Requirements**

**for the Degree of**

**Master of Computer Science at**

**Concordia University**

**Montréal, Québec, Canada**

**June 2020**

**© Jordan Terrence Crawford, 2020**

CONCORDIA UNIVERSITY

School of Graduate Studies

This is to certify that the thesis prepared

By: **Jordan Terrence Crawford**

Entitled: **3D Visualization of Hill-Sachs Lesions with Articulation**

and submitted in partial fulfillment of the requirements for the degree of

**Master of Computer Science**

complies with the regulations of this University and meets the accepted standards with respect to originality and quality.

Signed by the Final Examining Committee:

\_\_\_\_\_  
*Dr. Andrew DeLong* Chair

\_\_\_\_\_  
*Dr. Marta Kersten-Oertel* Examiner

\_\_\_\_\_  
*Dr. Olga Ormandjieva* Examiner

\_\_\_\_\_  
*Dr. Thomas Fevens* Co-supervisor

\_\_\_\_\_  
*Dr. Tiberiu Popa* Co-supervisor

Approved by

\_\_\_\_\_  
Lata Narayanan, Chair  
Department of Computer Science and Software Engineering

June , 2020

\_\_\_\_\_  
Amir Asif, Dean  
Faculty of Engineering and Computer Science

# Abstract

## 3D Visualization of Hill-Sachs Lesions with Articulation

Jordan Terrence Crawford

A Hill-Sachs Lesion is a wound to the humeral head that can result in shoulder instability and recurrent dislocation. The current standard for diagnosis and treatment is for the patient to undergo a CT or MRI scan of the glenohumeral joint. The attending physician then visually inspects the image slices to infer the actual damage to the Glenoid and humerus to then recommend a proper surgical procedure to correct it.

The treatment options for a Hill-Sachs Lesion vary in complexity, complication rate, chance of recurrence, and resulting joint mobility for the patient. Surgeons will diverge in their choice of correctional surgeries given the same set of CT/MRI images. This can result in a mismatch between the patient's actual needs and the chosen surgery.

We provide a 3D visualization and joint manipulation pipeline to increase the accuracy of diagnoses made by surgeons for treatment of Hill-Sachs Lesions. We transform 2D Dicom data into 3D space, where it may be posed and manipulated to give the surgeon a better view of the damaged site. We then introduce several convenience functions that solve for positions that are of interest when assessing the possibility of re-engagement and re-dislocation.

We also present the ability to position the 3D data at solved-for positions, and to make use of a calibrated VR orientation tool named Myo Bracelet to position and animate the humerus as if it were the patient's arm. We believe these steps allow simple and intuitive manipulation of the data that better represents the scenarios that surgeons visualize when planning their surgery.

# Acknowledgments

Special thanks to my supervisors, Tiberiu Popa and Thomas Fevens for being patient and allowing me to explore my research freely. Thanks also to professors Charis Poullis and Sudhir Mudur for their lively discussions. Paul Andre Martineau and Jimmy Tat for their consulting and participation in identifying the need and structure for this research. Lizhe He, Behnam Maneshgar, Vladimir de la Cruz, Prashant Raina, Xichen Zhou, Kaustubha Mendhurwar, Chen [Jocelyn] Qiao, Timothy Forbes and Qing Gu; for good input when talking graphics and for making a fun research atmosphere. Lastly, thanks to Mum, Dad, Shayne and Darien for their support while I finished this thesis!

# Contents

<b>List of Figures</b>	<b>viii</b>
<b>List of Figures</b>	<b>viii</b>
<b>List of Tables</b>	<b>x</b>
<b>List of Tables</b>	<b>x</b>
<b>1 Introduction</b>	<b>1</b>
1.1 Motivation . . . . .	2
1.2 Contribution . . . . .	4
1.3 Thesis Organization . . . . .	4
<b>2 Background</b>	<b>5</b>
2.1 Definitions . . . . .	6
2.1.1 Anatomical coordinate system . . . . .	6
2.1.2 Abduction . . . . .	6
2.1.3 External Rotation . . . . .	7
2.1.4 Horizontal Extension . . . . .	7
2.2 The Anatomy of a Hill Sachs Lesion . . . . .	8
2.3 The Glenoid Track . . . . .	8
2.4 Pre-operative Hill-Sachs Treatment Selection . . . . .	9
2.5 DICOM - Digital Imaging and Communications in Medicine . . . . .	12

2.6	Quaternions Applied to Visualization . . . . .	12
2.7	X-Ray . . . . .	13
2.8	CT Scan . . . . .	14
2.9	MRI . . . . .	15
2.10	SPECT scans . . . . .	16
2.11	Thresholding . . . . .	16
2.12	3D planning vs. 2D planning . . . . .	16
2.13	Meshes . . . . .	17
2.14	Marching Cubes . . . . .	17
2.15	Orientation Sensors . . . . .	18
<b>3</b>	<b>Workflow</b>	<b>19</b>
3.1	Choosing an Imaging Modality . . . . .	20
3.2	Animation . . . . .	22
3.3	Measures . . . . .	24
3.4	Displaying Impingement . . . . .	24
3.5	Calculating Engagement . . . . .	27
<b>4</b>	<b>Software Pipeline</b>	<b>31</b>
4.1	Software Program Pipeline . . . . .	31
4.2	3D Slicer . . . . .	32
4.3	Graphite and Meshlab . . . . .	33
4.4	OpenGL GUI and Interaction . . . . .	35
<b>5</b>	<b>Myo and Engagement Detection</b>	<b>36</b>
5.1	Clinical Manual Shoulder Diagnosis . . . . .	37
5.2	Method for re-orienting and displaying the points of interest . . . . .	37
5.2.1	Manipulating the Bone via Track Ball . . . . .	38
5.3	Myo Specs . . . . .	39
5.4	Manipulating the Bone via Myo . . . . .	40

<b>6</b>	<b>Conclusion and Further Avenues of Research</b>	<b>42</b>
6.1	Conclusion . . . . .	42
6.2	Limitations and Future Work . . . . .	43
6.2.1	Surgeon Survey . . . . .	43
6.2.2	MRI vs CT . . . . .	44
6.3	Graph Cuts . . . . .	44
6.3.1	Finite Element Analysis . . . . .	45
6.3.2	Myo Error . . . . .	46
<b>A</b>	<b>Bibliography</b>	<b>47</b>
<b>Appendix A</b>	<b>Appendix A - Code</b>	<b>53</b>
<b>Appendix B</b>	<b>Appendix A - Vicon Experiment</b>	<b>55</b>
B.1	Experiment Outline . . . . .	55
B.2	Data Post-Processing . . . . .	56
B.3	Discussion and Limitations . . . . .	58
B.4	Data . . . . .	59

# List of Figures

Figure 1.1	Anatomy of a Hill-Sachs Lesion [1]	2
Figure 2.1	MRI, Anatomical, and DICOM image Local Coordinate Systems[43]	6
Figure 2.2	Example of External Rotation[48]	7
Figure 2.3	Example of Horizontal Extension[32]	7
Figure 2.4	Anatomy and Typical Lesion Locations [47]	8
Figure 2.5	A Bony Bankart Lesion co-occurring with a Hill Sachs Lesion[38]	9
Figure 2.6	Latarjet procedure[5]	10
Figure 2.7	Illustration of a Remplissage Procedure.[46]	10
Figure 2.8	Engaging Hill Sachs Lesion [24]	11
Figure 2.9	X-Ray image of a Hill-Sachs Lesion with large bone loss [17]	14
Figure 2.10	Sample Visualization of 3D Slicer’s Marching Cubes Algorithm [4]	18
Figure 3.1	The edges of bone are blurred with soft tissue in MRI	21
Figure 3.2	View of the model showing chosen lines in purple	23
Figure 3.3	Initial View of the a Righthanded Glenohumeral Joint	25
Figure 3.4	Bringing the Lines to Parallel	26
Figure 3.5	Lesion in Critical Position, represented by red colored lines	28
Figure 3.6	Front View of the Critical Position	29
Figure 3.7	Another Possible Critical Position	30
Figure 4.1	An illustration of requirement compliance.	31
Figure 5.1	The Myo Armband [37]	39
Figure 5.2	Initial Myo Position	41



Figure 5.3	First calibration position . . . . .	41
Figure 5.4	Second calibration position . . . . .	41

# List of Tables

Table 5.1	Myo Specs	39
Table B.1	Frames	56
Table B.2	Frames Downsampled	57
Table B.3	Block 1	59
Table B.4	Block 2	60
Table B.5	Block 3	61
Table B.6	Block 4	62
Table B.7	Block 5	63
Table B.8	Block 6	64

# Chapter 1

## Introduction

In this thesis, we present research on 2D-to-3D visualization and animation of a glenohumeral joint and an open-source software pipeline for processing Dicom data. Our purpose is to help surgeons pose, reason, and plan about Hill-Sachs lesions(HSL) that go above and beyond traditional radiological techniques.

Shoulders are a complex net of sinew and muscle whose architecture gives us the greatest possible range of motion of all joints in our body. Complex structures break down in surprising and hard-to-imagine ways when subject to a destructive force. In particular, the shoulder joint can occasionally suffer a nasty one-two punch in the form of dislocations. This can leave it with lasting damage in the form of a HSL that is difficult for a surgeon to assess and repair.

The joint in the shoulder consists of three bones: the humerus, the scapula, and the clavicle. Normally, the spherical head of the humerus is nestled in a cavity inside the glenoid. This allows the shoulder to rotate freely. During dislocation, the humerus is either partially or completely popped out of the socket. In this paper, we examine the HSL. HSLs often occur during shoulder dislocation that happens in extreme sports like rugby, football, mountain biking, hockey, gymnastics, downhill skiing[13]. Since the forces involved in shoulder dislocation are so dramatic, the humeral bone and glenoid cavity are often damaged during either the initial dislocating event or the later shoulder reduction that returns the Humerus to its proper location.

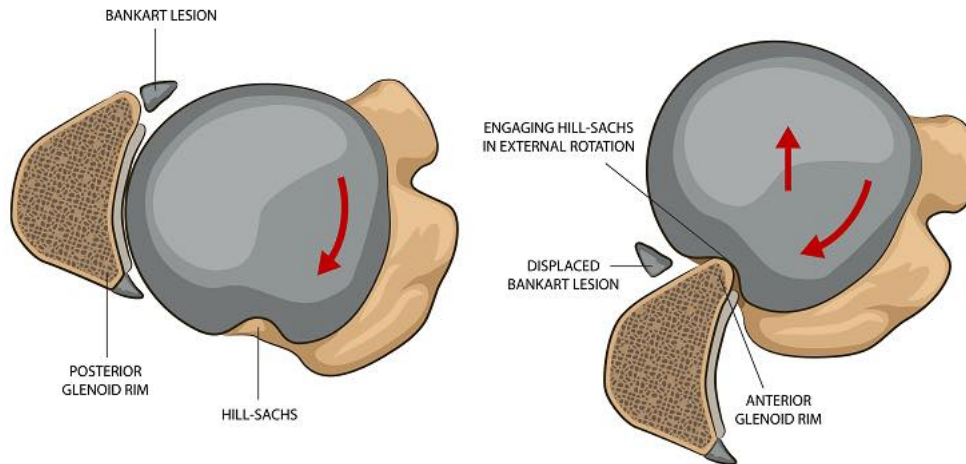


Figure 1.1: Anatomy of a Hill-Sachs Lesion [1]

The damage of interest to us can take the form of either a HSL or a Bankart Lesion. These lesions occur when a bone-on-bone impact possesses enough force to gouge away from the bone on either the humerus (HSL) or the glenoid cavity on the scapula. (Bankart Lesion) The probability of a shoulder dislocating increases after any kind of dislocation event (citation here). This is poorly understood, with diverse factors such as gender, tissue damage, and patient’s adherence to recovery exercises all playing a contributing factor [44].

## 1.1 Motivation

During the project, we spoke with a surgeon to familiarize ourselves more with the surgical field surrounding HSLs. He explained a particular class of stubborn and hard-to-treat patients that would return, sometimes multiple times over several years, with shoulders that dislocated repeatedly. There was the usual cadre of elite performance athletes, who could be expected to be at a higher risk for dislocation events. There were also electricians, motocross enthusiasts, and other seemingly “normal” patients as well.

He found that all of these patients shared HSLs in common. Identifying these lesions early on and taking them into account when making treatment decisions for the dislocation would make

for good prophylactic medicine. Indeed, there exist methods for diagnosing HSLs, as seen in [42] [21] which describe a percentage bone loss assessment technique. [49] describes a “Glenohumeral Track” technique for diagnosis.

During our talks, the surgeon outlined some weaknesses in these methods. He indicated that using losing strict bone loss as a criterion can fail to take into account the location of the lesion, which can affect their chance of re-engaging. For example, bone loss from a location on the humerus that sees heavy use, such as typing on a keyboard, falls within a much more frequently used range of motion than the bone loss suffered from a portion of the humerus that only does any work when scratching a stubborn itch in the middle of the back.

In the Glenohumeral Track, instead, a surgeon attempts to diagnose based strictly on the presence of a lesion in a generalized area on the humerus, this can also fail. The lesion may be shaped in such a way that there is a low chance of re-engaging it. The patient may also have a more specific range of motion that differs from textbook layout due to genetic or functional differences.

The stakes are high because surgeries come with drawbacks. Some of them sacrifice the mobility of the joint or introduce a serious risk of infection or rejection. Failing to appropriately treat a re-impinging shoulder can see the same patient returning to their attending physician a year later with the same problem.

In addition, doctors will often use 2D DICOM images taken from either a CT scan or MRI machine. The information is presented as a slide show of slices along one of three anatomical planes. This, and whatever proprioceptive feedback their patient gives, is their only view into what is essentially a dynamic 3D problem.

This is frustrating for all parties involved. At this point we, the computer scientists, figuratively raised our hands. Many algorithms have been developed in the field of Computer Graphics that facilitate the 3D modeling and posing of objects. We believe that these methods can be applied simply to implement a patient-specific wound modeling software that would allow more accurate planning and treatment of HSLs.

With this motivation in mind, we propose the following methods as contributions to the field of shoulder dislocation treatment:

## 1.2 Contribution

Our research demonstrates three main contributions. The first is the design and use of a suitable approximation collision construct to simulate and detect potential Hill-Sachs Engagements for a particular patient's data set. This detection is indicated to the user and is record-able. We hope that with the ability to view and articulate this data, surgeons will be able to be trained to use our tool to reason more consistently about the specific geometry and dynamics involved in an engaging HSL.

The second contribution is a calculation that automatically positions the humerus in a potential problem position and indicates to the user that the shoulder has the potential to impinge at that location. This can be used in conjunction with a click-and-drag feature that allows the user to move the bone around the problem position to get a better sense of the realism of the position.

The final contribution is a calibration procedure for allowing the inputs from a VR Myo bracelet to be used when placed on the bicep of the user. This function allows the user to move the humerus as if it were their own, to explore the realism of the impingement possibility themselves.

## 1.3 Thesis Organization

We will present some background research that is representative of the computer vision and graphics techniques that we used while implementing the custom elements of the pipeline. Additionally, contextual information will be provided for readers unfamiliar with medical terminology and research related to the Hill-Sachs 3D Visualization problem.

This will be followed with a description of the methods we used to prepare the data, mathematical equations that were used, and software features that we wanted in the final pipeline.

Next, the actual full software pipeline that was coded from scratch will be shown and explained. This will include top-level descriptions of the features we used from 3D Slicer, MeshLab, and the Myo motion detection features we used to help pose our objects.

The thesis will be concluded with a discussion of the experiments and challenges faced during research/programming, as well as a short discussion of future avenues of research that the tool may be employed in.

## **Chapter 2**

# **Background**

As noted earlier, the background will include a survey of information and research to lay the groundwork for understanding the medical terminology and computer processing algorithms that form the backdrop of our Hill Sachs Visualization Pipeline.

We begin by describing the surgical options that our pipeline helps to decide between. This is followed by a description of 2D imaging modalities that surgeons will typically use to help explore the wound site. Finally, the segmentation and mesh reconstruction techniques that are available to bring information from 2D modalities into the 3D analysis.

## 2.1 Definitions

### 2.1.1 Anatomical coordinate system

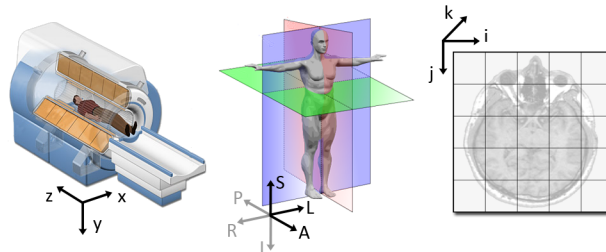


Figure 2.1: MRI, Anatomical, and DICOM image Local Coordinate Systems[43]

Several coordinate systems are commonly used in the medical domain. When referring to anatomy, the terms Left, Right, Anterior(front), Posterior(back), Superior(up) and Inferior(down) are used. To describe a particular coordinate system, one may pick three of these directions to name the positive  $x/y/z$  axes of the system. For example, Left Posterior Superior would denote X-values that increase while moving left, Y-values that increase while moving backward, etc.

### 2.1.2 Abduction

This is a movement away from the mid-line of the body. Moving from a neutral arm position to a horizontally extended arm position would be an example of abduction.





Figure 2.2: Example of External Rotation[48]

### 2.1.3 External Rotation

This refers to rotation away from the body. In the context of the shoulder joint, it refers to a motion of the arm that extends the arm above and out relative to the torso.

### 2.1.4 Horizontal Extension

This refers to a straightening of the two parts connected to a particular joint in the horizontal plane of motion.



Figure 2.3: Example of Horizontal Extension[32]

## 2.2 The Anatomy of a Hill Sachs Lesion

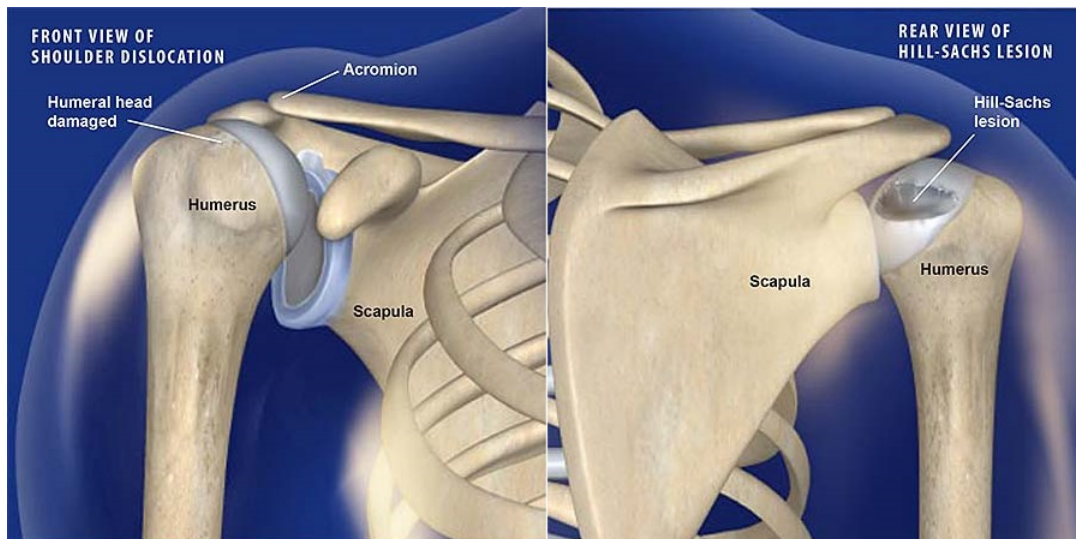


Figure 2.4: Anatomy and Typical Lesion Locations [47]

The original description of the Hill-Sachs Lesion describes it as a defect located posterior and medial to the greater tuberosity on the posterolateral aspect of the articulating surface of the humeral head. The groove is navicular or wedge-shaped and its average measurements are 2.5 cm in length, 1.5 cm. in width, and 0.75 cm in depth. The lesion is demarcated from the surrounding normal bone by sharp or vertically projecting walls of bone, which in the larger defects stand at a right-angle to each other. The spongy bone bordering the defect is thicker than elsewhere and is covered with a glossy, smooth connective tissue layer[26]. Further, Hill-Sachs lesions exist in the area between 0 and 24 mm from the top of the humeral head. [39].

## 2.3 The Glenoid Track

The presence of a lesion does not mean that it will interact and cause discomfort or recurrent dislocation. In medical literature, one of the standards for assessing whether or not a lesion will result in future shoulder instability is the idea of the “Glenoid Track”.[49] describe a study where cadaveric joints were examined and manipulated to map a subset perimeter along the humerus that corresponds to the interaction of the glenohumeral joint during normal motion.

They qualify the limits of normal motion as the range with the arm in maximum external rotation, horizontal extension, and 0/30/60 degrees of abduction. These reference points are used because most everyday movement occurs within this range, and lesions that occur inside the Glenoid Track are more likely to engage than ones that occur outside of it.

Ordinarily, the joint contact surfaces in the shoulder have a layer of articular cartilage that allows them to move smoothly in the joint. When damaged, they lose this protective layer at the site of the injury. This creates the potential for painful bone-on-bone contact. In instances of more severe Hill Sachs Lesions, there is enough bone loss for the edge of the Glenoid to become caught in a trough in the damaged Humerus. This phenomenon is termed “engagement” of the Hill Sachs Lesion.

The patient’s joint becomes locked, and efforts to reverse the engagement can cause further damage to the bone as the bone/bone surface scrapes material off on the way out. It can also cause re-dislocation events that cause a return to the hospital where the surgeon is faced with a more damaged shoulder than was previously treated [12]. The position, orientation, and degree of bone loss in a Hill-Sachs Lesion all influence the likelihood of the two bones engaging. Lesions that are wedge-shaped present the highest chance of causing engagement.

## 2.4 Pre-operative Hill-Sachs Treatment Selection

There exist a multitude of surgery choices for treating unstable shoulders, and when polled most surgeons have a preferred surgery when the injury has particular characteristics. [20]

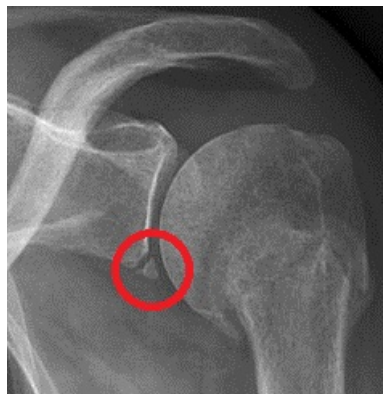


Figure 2.5: A Bony Bankart Lesion co-occurring with a Hill Sachs Lesion[38]

An injury that often co-occurs with the Hill-Sachs Lesion, and also forms the focus of some of the treatment options available for the Hill-Sachs is the Bankart lesion. This lesion can occur in soft tissue and bony variants, and linear damage to the glenoid. Apart from causing significant discomfort to the patient, these cases can cause further damage to both the humerus and glenoid[7].

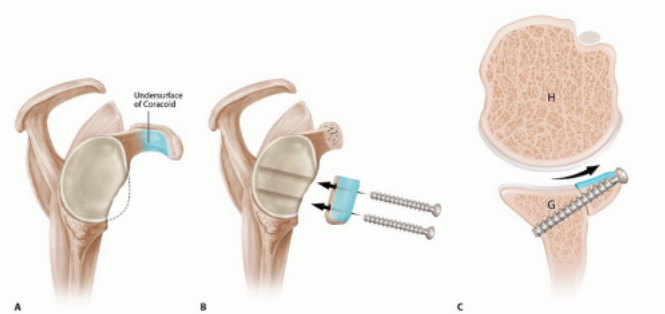


Figure 2.6: Latarjet procedure[5]

Latarjet [42] fixes the instability associated with both minor Hill Sachs Lesions, characterized as greater than 20% bone loss, and Bony Bankart Lesions at the same time. It consists of augmenting the glenoid cavity with a bone graft sourced from either the patient or a cadaver. This surgery has a high success rate in preventing recurrent dislocations. It has a higher complication rate than other surgeries due to possible rejection of the bone graft or infection of the wound. It also results in a more restricted range of motion than was available to the patient pre-injury. This can be of great importance to athletes in sports like Rugby, where the newly restricted range of motion in the Glenohumeral joint can prevent or limit a throwing motion.



Figure 2.7: Illustration of a Remplissage Procedure.[46]

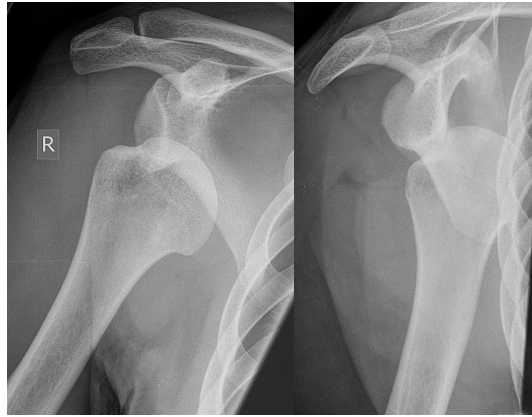


Figure 2.8: Engaging Hill Sachs Lesion [24]

Remplissage [42] is done when there is an even greater degree of bone loss. It pins the tendon along the anterior side of the humerus, preventing the shoulder from reaching the problem angle. This solution removes the problem entirely, but restricts movement even more than the Latarjet does, making it very undesirable for patients that make use of the functional positions that become impossible post-surgery.

For patients aged 20-35 presenting with general shoulder instability, many surgeons will prefer to treat the shoulder using either an open or arthroscopic Bankart repair surgery. When asked about their choices for situations that feature bone loss on either the glenoid or both glenoid and humerus, they favored the more involved Latarjet or Remplissage procedures. Thus, successfully identifying the situation and type of damage is an important step in selecting an appropriate surgery

The benefits and drawbacks of the different surgical options necessitate due consideration on both the part of the patient and the surgeon. Pre-operative analysis of CT, radiography, MRI, and Ultrasound data are thus all important tools and options for a surgeon to consider when choosing and planning a surgery that best suits the patient's needs.

In the case of a Hill-Sachs Lesion, an additional factor plays a role: the “engagement”- of the lesion. Engagement is caused by the troughs carved in the humerus getting caught on the edge of the glenoid socket. Patients with an engaging lesion sometimes return with re-dislocations, or with their arm stuck in the pose which their shoulder engaged in.

In the literature, HS lesions are characterized by percentage bone loss[14] and 2D CT or MRI

images. This information is used to inform the risk profile of different surgical treatment options. In this paper, our goal is to amplify the array of tools presented to the surgeon while diagnosing and considering treatment solutions. We argue that the HSL re-engagement factor can be characterized more accurately by first re-visualizing the 2D information into 3D, and then adding a simple geometric measure that captures orientation and proximity information that is lacking in traditional analysis.

## 2.5 DICOM - Digital Imaging and Communications in Medicine

DICOM is a medical image format a header specified by a 128 byte File Preamble and a 4-byte Prefix. The header features space to include patient, imaging, and treatment data. Because of this, the file needs a viewer that is capable of interpreting the header data block before displaying the image. Standard image viewers will display pixelated junk data. This necessitates the use of a viewer capable of parsing the header and properly displaying any image data available. Additionally, the data sets for our research involve the viewing of multiple ordered Dicom slices. They come with a metafile that specifies the number and order of the images for a particular folder. Given these requirements, our viewer also needed to be able to parse the meta-files to show the familiar slide-show view that many surgeons rely on.

## 2.6 Quaternions Applied to Visualization

The orientation of the Myo bracelet is output continuously as a Quaternion. Quaternions are an alternate way of representing a rotation with properties that are advantageous when performing rotation interpolation, or for high-volume continuous updates. For convenience, we adopted the same Quaternion notation for our local coordinate systems. We quickly present a short breakdown of some basic properties that Quaternions possess that we make use of in our calculations.[23] [41]

A quaternion  $q$  is a 4-tuple

$$\tilde{q} = q_0, q_1, q_2, q_3$$

$$\tilde{q} = (q_0, 0, 0, 0)$$

$$\begin{aligned}
s &= q_0 \\
\tilde{q} &= (0, q_1, q_2, q_3) \\
\bar{t} &= \text{vec}(\tilde{q})
\end{aligned}$$

Where  $s$  is the scalar part denoted by  $q_0$  and  $t$  is the vector part denoted by  $(q_1, q_2, q_3)$ . This allows a more compact notation when compared to the 3x3 matrix notation, and requires only 4 floating point updates compared to the 9 that a matrix representation requires.

A 3-vector can be written with quaternion notation by denoting a 0 scalar part. Quaternions can be used to represent rotation about an axis (denoted by the unit vector  $k$ ) by an angle  $\theta[-\pi, \pi]$  as follows

$$\tilde{q} = \cos(\theta/2) + \bar{k}\sin(\theta/2).$$

Multiplication of two quaternions  $p$  and  $q$  is given by

$$p * \tilde{q} = p_0q_0 - p * q + q_0p + p_0q + p \times q$$

Given a quaternion  $\tilde{q}$ , its conjugate  $\tilde{q}^*$  can be written as:

$$\tilde{q}^* = (q_0, -q_1, -q_2, -q_3).$$

If the scalar part of a quaternion is 0,

$$\tilde{q}^* = -\tilde{q}$$

The conjugate has the following property:

$$\text{vec}(\tilde{q}\tilde{q}^*) = 0$$

## 2.7 X-Ray

The first line of imaging for this domain is often the X-Ray, a 2D image generated using projection radiography[11]. It functions by passing 10 to 100 keV wavelengths through the body part being imaged. Wavelengths in this range are absorbed more readily by denser tissues, such as bones, than by the softer surrounding tissues.



Figure 2.9: X-Ray image of a Hill-Sachs Lesion with large bone loss [17]

The scans are done quickly, and in the context of the HS lesions, serve to give a broad estimation of potential damage in the shoulder. Unfortunately, the fundamentally 2D nature of this kind of imaging can lead to an obscured view of the injury, depending on the chosen imaging plane. Our pipeline aims to take advantage of imaging techniques that translate more easily into 3D.

## 2.8 CT Scan

Computer tomography images are crucial to modern radiology. Their inception dates back to 1917 when the Austrian mathematician Johann Radon developed his eponymous transform. He came up with a mathematical proof that a function could be expressed as an infinite set of its projections [36]. Following this was a paper treating a method of finding approximate solutions to large systems of linear algebraic equations [27]. The technique in this form spent a long while unused,



until a period of work during which these techniques were rediscovered[33] and developed them into the first CT machine.

The ACTA was the first full-body version of the CT scanner that did not require extraneous equipment[40]. It functioned by shining a thin diameter ray through the body in a translation/rotation motion, and then sampling the X-rays after they have passed through the tissue. Different tissues have different absorption profiles, and the differences can be resolved into an image using the mathematic techniques discussed earlier. Each tissue is given a Hounsfield unit number that represents this varying absorption, with distilled water serving as 0 units. The ACTA produced a 160x160 resolution image, with each element in the image corresponding to a 1.5mm cross-sectional area. Over time, CT imaging technology was refined to produce the sharper images that we use as input into our pipeline.

CT scanners output grayscale images. The format specifies the field of vision that the scanner images. It has height, width, and depth. The first two are shown directly, and the third is specified as a slice depth. The millimeter-scale is used, with slices depths varying between 0.2mm and 1.0mm. Those with sharp linear gouges situated medially on the humeral head and those cases where the bone loss is significant are more likely to re-engage than otherwise. [21]

## **2.9 MRI**

Magnetic Resonance Imaging is another diagnostic imaging modality present in the field. It functions by rapidly switching the gradient direction of a magnetic field at an extremely fast rate. Because protons are electrically charged, and due to the relation between the electrical and magnetic forces, protons are subject to influence by this magnetic field.

MRI is an imaging modality that is primarily used in the diagnosis of soft tissue diseases[29] and is ill-suited for imaging bones because it has better contrast and field-of-view focus when used to image tissues that have a higher hydrogen content.

## 2.10 SPECT scans

SPECT is an acronym for Single-photon emission computed tomography. It uses a combination of an injected radionuclide that binds to a particular tissue of interest and a gamma camera to visualize true 3D information[28]. It is uncommon to use SPECT scans to query cases of HSL because the damage is on the bone, which has a poor rate of uptake for radionucleotides and is best visualized using other imaging techniques.

## 2.11 Thresholding

Thresholding is an analysis of image pixel intensities based on the choice of a threshold value. One use of thresholding is to separate and classify pixels into background and foreground elements based on this value to create a segment that contains a region or feature of interest in the foreground.

Such methods are sometimes automated and applied to medical image data[35]. They are the most basic way to segment images and are extremely simple to implement and use.

## 2.12 3D planning vs. 2D planning

Taking 2D data and transforming it to 3D to clarify diagnoses is an established idea in the medical field. It isn't often that people ask whether or not this helps surgeons make their decisions more efficiently. Rather, it is assumed that 3D is closer to what we encounter every day and so this assumption must hold when supplying novel visualizations to help planning.

In reality, the truth is somewhat more nuanced. [22] Found that some benefits were indeed accrued for inter and intra-observer reliability, but that younger residents benefited more from the novel method.

The reason to make the jump from 2D to 3D becomes clearer when interobserver biases between surgeons in their diagnoses are examined, as in [8]. These authors found that even among different 2D modalities of different resolution, significant differences in surgeon diagnoses could be observed. We posit that a similar pattern holds between the jump from 2D to 3D for HSL, with 3D presenting far clearer and more useful surface information than 2D for surgeons on the lookout for

novel diagnosis techniques.

Indeed, the preoperative prediction of the engagement of the HSL, based on findings that engaging HSL was larger and more horizontally oriented to the humeral shaft than non-engaging lesions[14], as presented in 3D visualizations, is useful in planning additional procedures to treat a significant bone defect on the humeral head.

## **2.13 Meshes**

Meshes are a common way in the computer world of visually representing and manipulating 3-dimensional shape information. They consist of vertices, which are points in a 3D space; edges, which represent connections between vertices; and faces, which are surrounded by vertices and edges [19]. Together, they form a graph data structure that may be traversed from vertex to an edge to a vertex. Observations and equations may be applied along the way to reason about the geometry of the object.

## **2.14 Marching Cubes**

Marching cubes is an algorithm that creates triangle polygonal mesh data of constant density surfaces[30] from 3D data. Using a divide-and-conquer approach that observes pixel data to generate inter-slice connectivity, a mesh topology that reflects the 3D surfaces present in the pictures can be created. The algorithm processes the 3D medical data in a scan-line order and calculates triangle vertices using linear interpolation. The algorithm can typically include another pass that observes the gradient of the edges it generates to use as a basis for surface normals that can be used to shade the models.

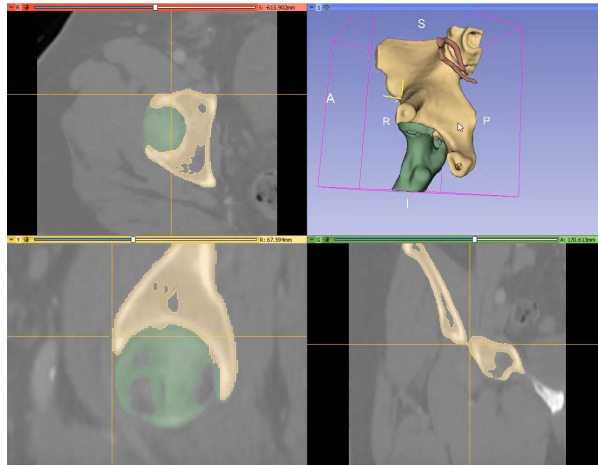


Figure 2.10: Sample Visualization of 3D Slicer’s Marching Cubes Algorithm [4]

3D visualization is becoming a popular method of visualizing data to plan surgeries in hospitals [45] Images of these surfaces, constructed from multiple 2D slices of CT , MRI and SPECT, is a cheap way[25] to help physicians understand the complex anatomy present in the slices. Interpretation of 2D medical images requires special training, and although radiologists have these skills, they must often communicate their interpretations to the referring physicians, who sometimes have difficulty visualizing the 3D anatomy.

## 2.15 Orientation Sensors

A variety of sensors have become widely and cheaply available on the market.

Magnetometers can sense the magnitude and direction of magnetic fields, including the Earth’s magnetic poles. A compass is a very basic example of a Magnetometer.

Accelerometers measure absolute changes in acceleration, often using the Earth’s gravity along with other Accelerometers as a reference to reason about its absolute acceleration in Earth’s coordinate frame.

Vibrating Gyroscopes can be used to make orientation measurements due to the way a force on the support of a vibrating object behaves when subject to an orientation change.

Such sensors are sometimes combined in 3-axis units on computer chips as an Inertial Measurement Unit (IMU). Such sensors allow orientation measurements in free space.

## Chapter 3

# Workflow

Here we describe the process of obtaining the final basic workflow for our tool. We speak about our interview with an orthopedic surgeon and our literature search, and how it arrived at a possible inter-observer bias in standard HSL diagnosis. We then postulate that this bias could be minimized by introducing graphical elements and control schemes that allow a better sense of the data.

We began by interviewing a surgeon, Dr. Paul Martineau, versed in our area of interest: the orthopedics of the shoulder. He described his view of modern treatment guidelines for HSL across North America and Europe. He emphasized a tendency for surgeons to prescribe conservative treatments [20] that result in avoidable loss of range of motion in athletes.

The next step up was the concept of the glenoid track [16], where treatment strategies acknowledge a geometrical element in their application. Together, we posited that a more complete criterion would describe the HSL in terms of its physical shape. Such a criterion would allow a surgeon to distinguish lesions that were likely to engage from non-engaging lesions, a feature absent from the most common approaches in the field.

It was mentioned that surgeons would typically apply these concepts while observing 2D images in the form of either a CT scan or an MRI scan, depending on what was available for the patient.

This methodology is less sound than it could be. The analysis of 2D images is vulnerable to inter-observer variation. This means that two surgeons with similar backgrounds can interpret the same HSL differently when observing the same data. This allows for the possibility that the same patient would receive different treatment given two different surgeons, with one treatment being the

inferior option [8]. The study notes that CT data provides more consensus than radiographs when both depict the same lesion, which leads us to posit that the increased clarity of the site of injury in the CT images leads to more consensus among surgeons, and thus higher diagnostic accuracy.

A way of further increasing the clarity of the site of injury is to process the 2D slices into a 3D mesh representation using the marching cubes algorithm [30] and basic graphics display techniques. Then, equipped with this new; better view of the data, any problems with the glenohumeral joint anatomy would be anatomically clear to a viewing surgeon.

### **3.1 Choosing an Imaging Modality**

The availability of data presented us with two candidate imaging modalities: CT and MRI. We obtained sample data for HS lesions by contact with Dr. Martineau. This comprised an initial 7 cases, 3 of which contained both MRI and CT scans. All 7 were fairly severe lesions. Data was non-uniform, with slice counts numbering between 12 and 250 slices.

On perusal of the data, we noted that the MRI images tended to have bone boundaries with lower quality boundaries than their CT counterparts. These were due to the specs (1.5 Tesla vs. 3.0 Tesla) of the machines being used, of which the MRI was of lower quality. MRI machines have many parameters that are tuned when scanning the patient, and these images showed the telltale signs of tuning for soft tissue structures.

Indeed, MRI is commonly used for analyzing soft tissue structures while the hard-tissue contrast for CT is easier to work with for bone segmentation. This is evidenced by research aimed at co-registering MRI/CT [15], where the different information of the two techniques is combined to better plan rectal cancer surgeries.

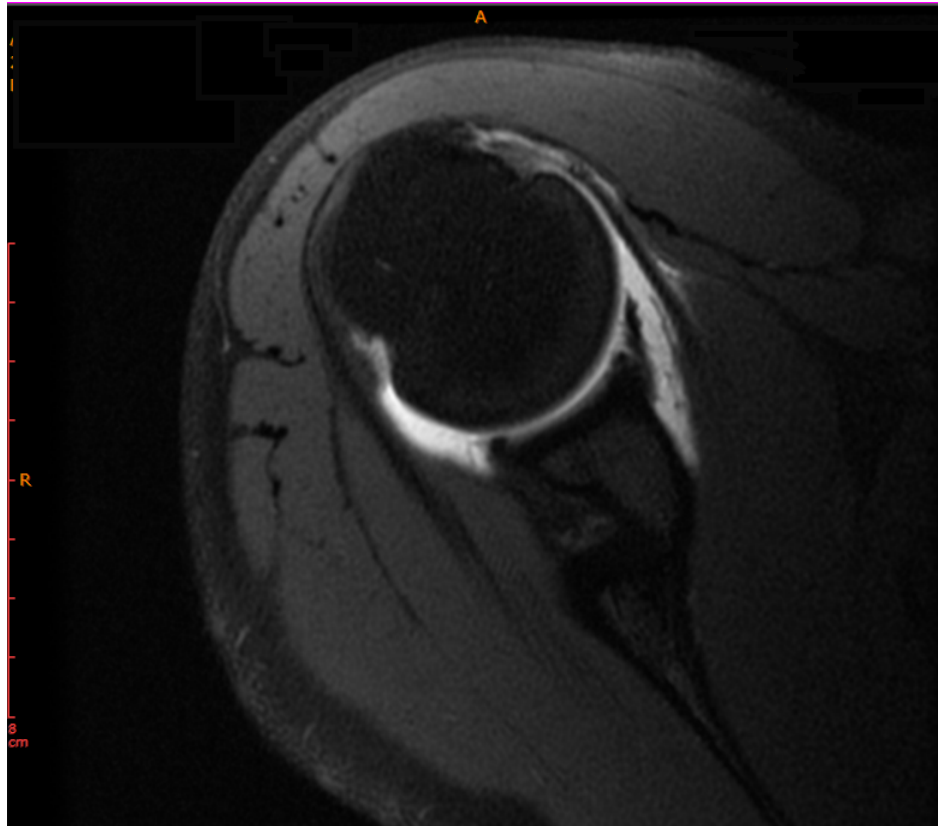


Figure 3.1: The edges of bone are blurred with soft tissue in MRI

These structures are often good views of the tendons, cartilage, and swollen tissue in the area. The tendons don't play into the diagnosis of the HSL, because the bone mechanics are more dominant of a factor for whether or not the shoulder will re-dislocate. They have some bearing on the choice of surgery, because tendon repair needs to be addressed at the same time as the humeral bone defect. While important components, they regrettably obscured the bone in many of the slices, the most pertinent part.

We decided to choose CT, which had sharper boundaries due to a higher resolution and a clear greyscale focus on the bone.

Once visualized and accessible, we outline and propose some features that allow the articulation of the Glenohumeral joint.

## 3.2 Animation

First, we add a drag and drop style tool centered around the joint. By clicking and dragging, the user can change the rotation of the bone about the socket.

**Local Coordinate System Picker** Once the bones are placed in a viewable location, the focus rapidly shifts to the lesion itself.

One approach to dealing with the engagement of the lesion would be to use a full mesh-to-mesh collision simulation, or some form of finite element analysis as in [31], and then subjecting the bone to simulated physical forces until an engagement was observed.

In such a simulation, the force dynamics involved are poorly defined when the source information is only a CT image. The bone surface in our data was not smooth on the fine-scale, which could lead to over-corrections in a hypothetical collision engine. Additionally, soft-tissue plays a significant role in the full picture of the forces that a humerus is subject to. A lack of cartilage can misrepresent the surface, and a lack of tendons could result in unrealistic trajectories for the bone on their way to a target position. Such approaches[9] are certainly valid in other contexts where the provided data can offer approximations to all of the above and have been successfully used to study the outcomes of full shoulder reconstruction.

While these more complicated physics representations exist, our view is that we would always fall shy of a proper bone and soft-tissue physics model of the joint, given our data. Thus, our preference is to allow model inter-penetration and leave it to a surgeon's verification to determine if the position we solve for is unrealistic given the underlying human anatomy.

The question becomes: How simple?

Any kind of simplification requires 1. That the wound be represented by a suitable approximation that captures the essential characteristics of the HSL. 2. The movement of the bone should be described by realistic assumptions

We reasoned that the central lines of both the HSL and either the accompanying Bankart lesion or the likeliest edge of the glenoid cup, were the most likely to interact in the case of impingement. To represent these lines, we chose four anatomical landmarks. This was because . Two of the landmarks are placed by the surgeon at either end of a centrally representative line of the lesion. An



additional two that will be used to denote a similar line along the interacting section of the glenoid cup. The general heuristic for selecting this line is to find the damaged piece of the bone. The damage usually presents as a chipped surface. Selecting the two most extreme points around the damaged area results in the most likely surface for the bone to interact with.

On selecting the option, the user is prompted to pick a new Hill-Sachs line and Bankart line by clicking a series of 4 points on the bone wound exteriors. On completion, these lines will be displayed in purple.

Our program provides a utility that indicates when the lines occupy an orientation and position that is likely to result in impingement. We posit that the lines must necessarily be both close and within a degree of being parallel for a locking event to occur.

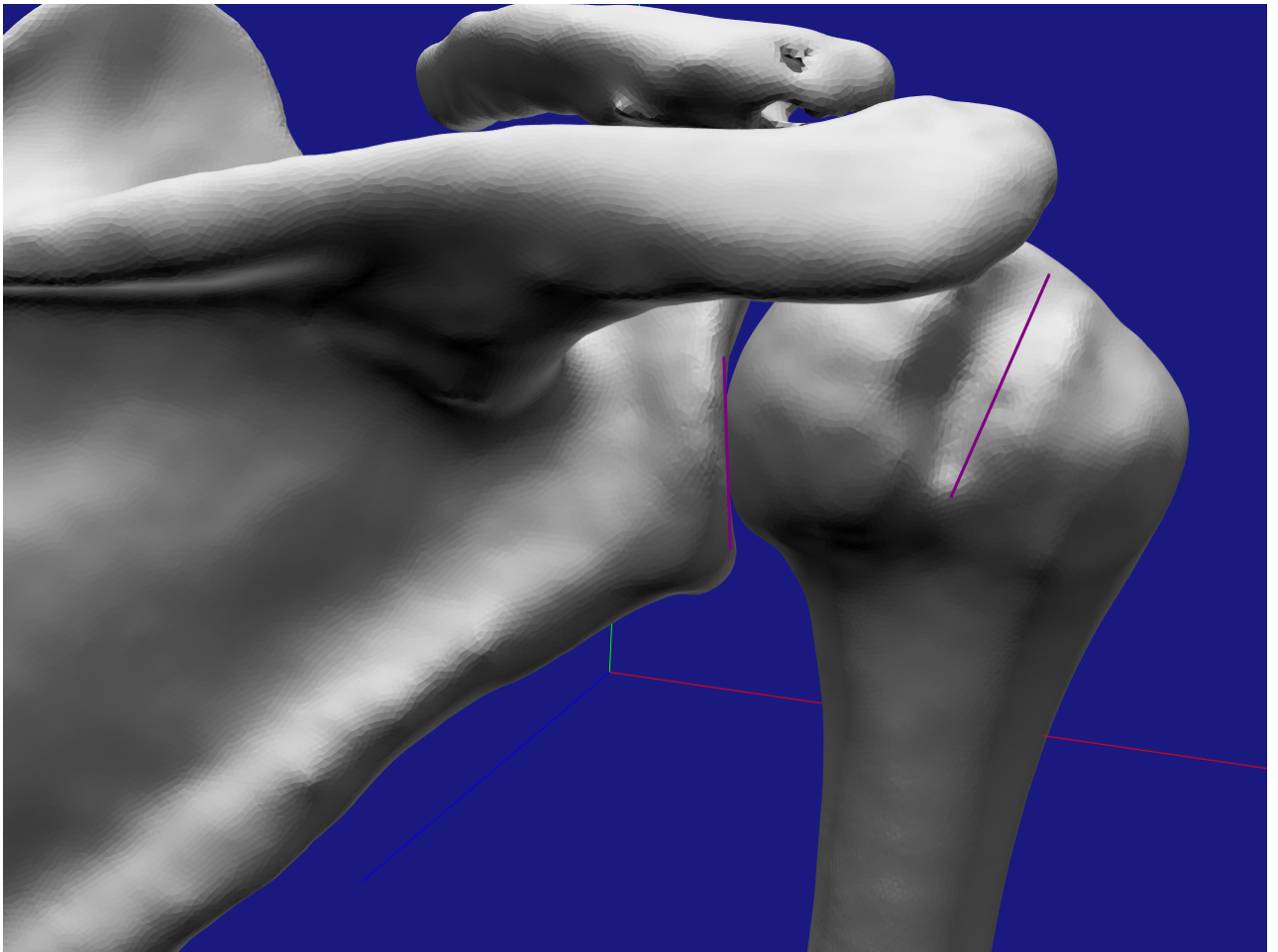


Figure 3.2: View of the model showing chosen lines in purple

### 3.3 Measures

#### Translation Measure

$$T = \frac{(p2+p1)}{2} + \frac{(p3+p4)}{2}$$

One of the necessary preconditions that we posit must be true before an impingement is possible is positional proximity. The center of the lesion must be close to the edge of the glenoid. To measure this, we take the midpoint of the humeral line, defined by p1 and p2, and compare its position with that of the glenoid line's midpoint, defined by p3 and p4. If they are within 1% of the bounding area, we say that the precondition of proximity is true.

#### Rotational Measure

$$R = \arccos \frac{a \cdot b}{\|a\| \|b\|}$$

The second necessary precondition is that the lesion and glenoid must be close to parallel for an impingement to occur. Else, the humerus will tend to interact normally. To measure this, we take the arc cos of the dot product of the two approximating lines, represented by a and b. If the lines differ by less than 2 degrees, we say that the HSL and the colliding edge of the glenoid cup are aligned, and thus an impingement between the two is possible.

### 3.4 Displaying Impingement

Another function sequence of G, H and then J key performs a rotation that makes the lines parallel, calculates a rotation that places the center point of the line at the closest section to the other line, and then lets you jiggle the line to see orientations close to the triggering one.

We provide another function that places the HS lesion in the closest impingement configuration possible with regards to the chosen B line. In the first step, a dot product is performed to yield the rotation to bring the lines parallel. In the second step, an axis is calculated that, when rotated around, will leave the two lines parallel. Along the rotation path, is a single angle theta that results in the best possible score for both rotation and position measures. We recognize that the HS lesion

can “fall into” the interacting region, so we also allow the user to rotate freely around the calculated axis to few other possible nearby orientations that can also result in impingement.

Saving and sharing orientations of interest are also allowed in our program. The present position and orientation of the humeral bone can be output to a file and reloaded for later viewing.

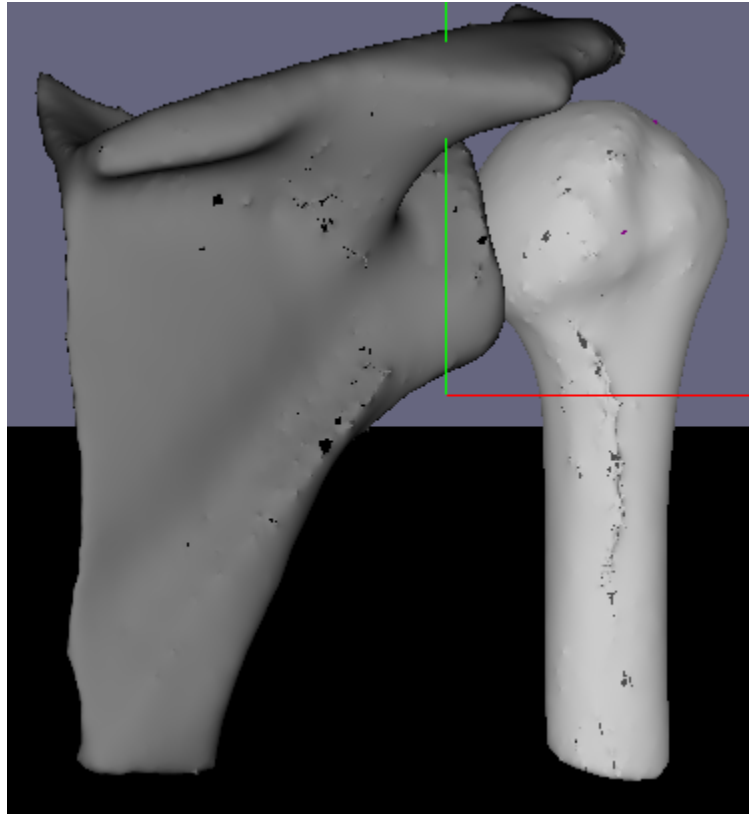


Figure 3.3: Initial View of the a Righthanded Glenohumeral Joint

Here we see the initial alignment of a dataset featuring the right shoulder of a patient that received a CT scan whose cross-section includes the glenohumeral joint; the focus of our efforts.

We calculate the centroid of the mesh and display the entire model centered at the origin, with several colored axes denoting the  $x/y/z$ -axis. This allows some additional reference by introducing some landmarks. We found that this allows the user to keep a better orientation when manipulating the model.

Here we made a function to toggle the transparency of the model to allow viewing of the lines that demarcate the HSL more clearly, otherwise, the lines tend to be obscured by the mesh. This

is done by lowering the alpha value in the shader to a value of 0.7 for the bones while keeping the value of the line full.

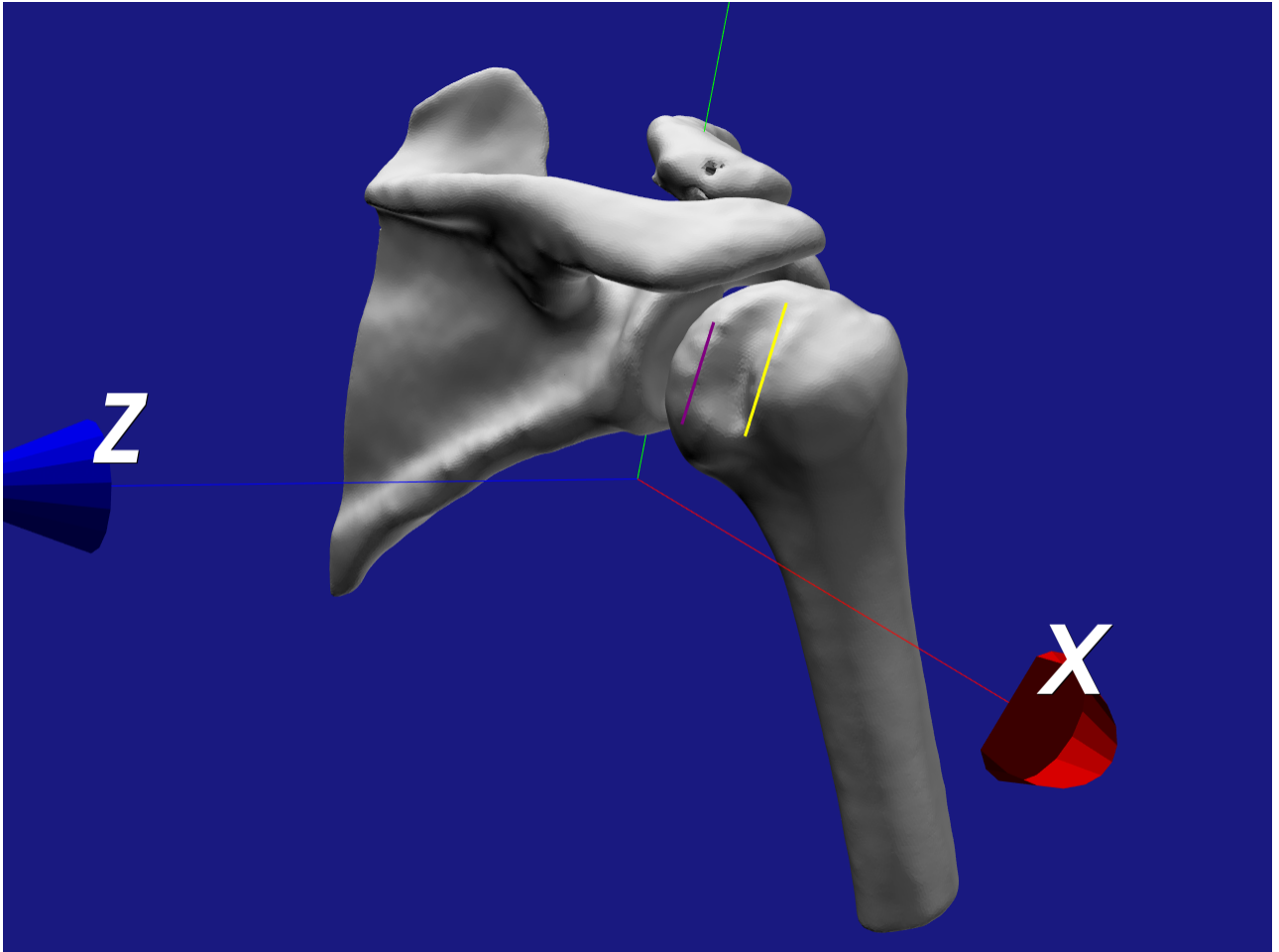


Figure 3.4: Bringing the Lines to Parallel

We aim to find the orientation of the humerus that most closely aligns the lesion with the apparent interacting edge of the glenoid joint, because this represents the final physical position of the humerus impinged on the glenoid. One technique is to calculate rotation and translation that causes the two lines to coincide.

However, there is very little translational motility in the shoulder joint. This is because the joint structure is generally held in place by the system of tendons, and the interacting cartilaginous surfaces in the joint don't deform to a large degree.

Given that our goal is to achieve a simple visual estimation that closely resembles the true configuration in a live shoulder joint without relying on collision physics, we discard the small translational component in favor of focusing on the rotational component. This simplification allows a rapid calculation by inspection of possible problematic positions.

To account for this, we attempt to find, using only a rotation, the alignment of the representative lines that bring the centers of these lines closest together.

As our first step, we affix the two lines to be parallel by calculating the dot product between the two. This allows us to restrict the remaining rotation that minimizes the distance between the two lines to a single variable rotation along an axis that preserves the parallel nature of the lines.

### **3.5 Calculating Engagement**

After the mesh is mobile, there is the question of which positions are liable to cause a re-engagement problem. In our earlier anecdote of the patient on the table, the patient's discomfort was the cue used to assess which positions were an issue. Lacking this cue, we would like to simulate it by developing a condition under which we declare impingement to be likely or detected.

This pose of impingement can be detected and displayed using a two-step calculation. In the first step, we simply calculate the dot product between the two lines and perform the rotation that causes them to coincide. This minimizes the rotation measure. In the second step, we preserve this angle and perform a parameterized rotation about an axis defined as the cross product between the two vectors pointing from the center of the anatomical landmark lines to the center of rotation of the humerus. This ensures that the lines do not lose their orientation as they are manipulated toward one another. After this, we simply choose the location that provides the minimal distance between the centers of the lines given these restrictions.

Once the lines are brought into alignment, we visually indicate this fact by coloring the lines red.

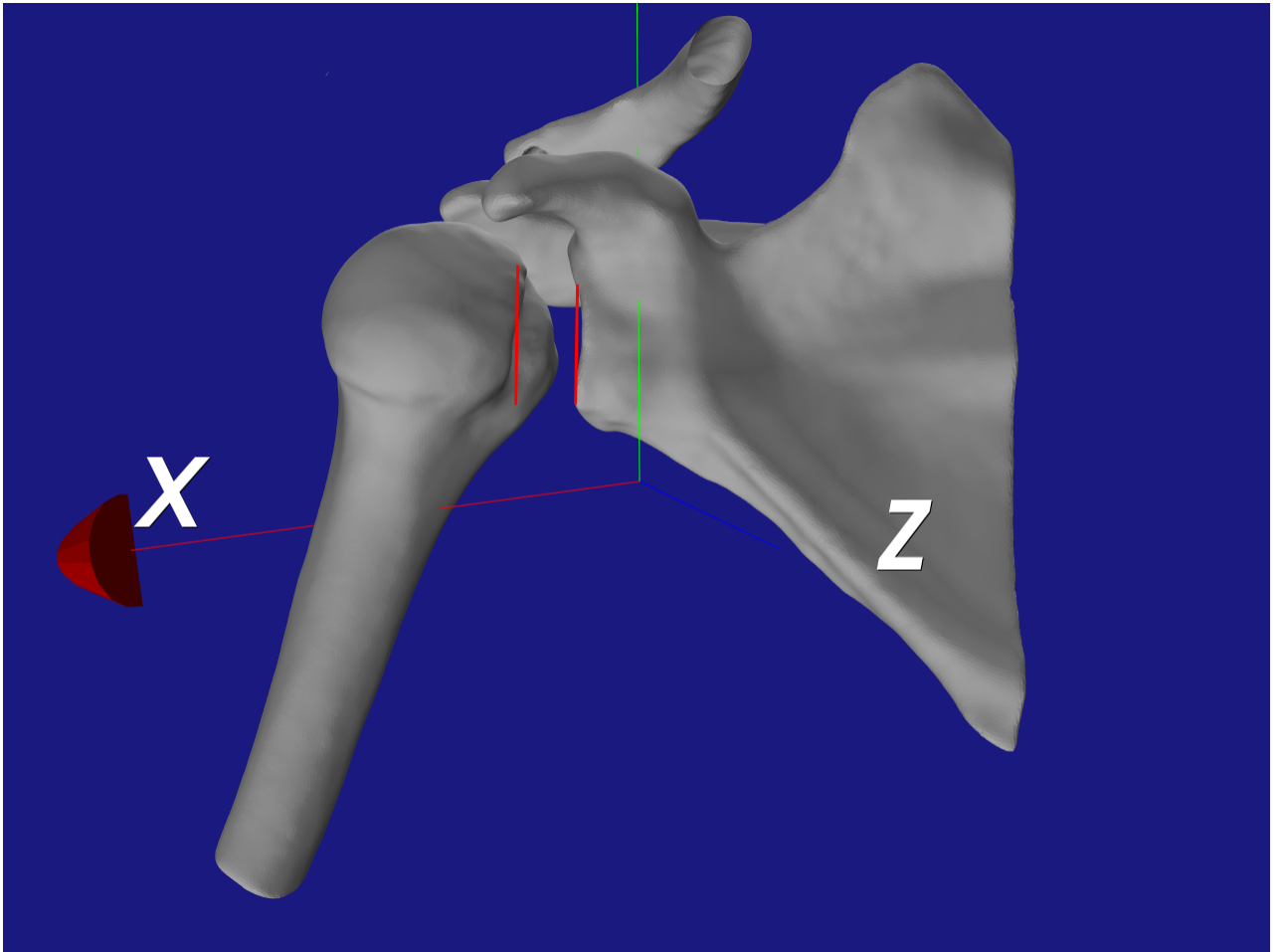


Figure 3.5: Lesion in Critical Position, represented by red colored lines

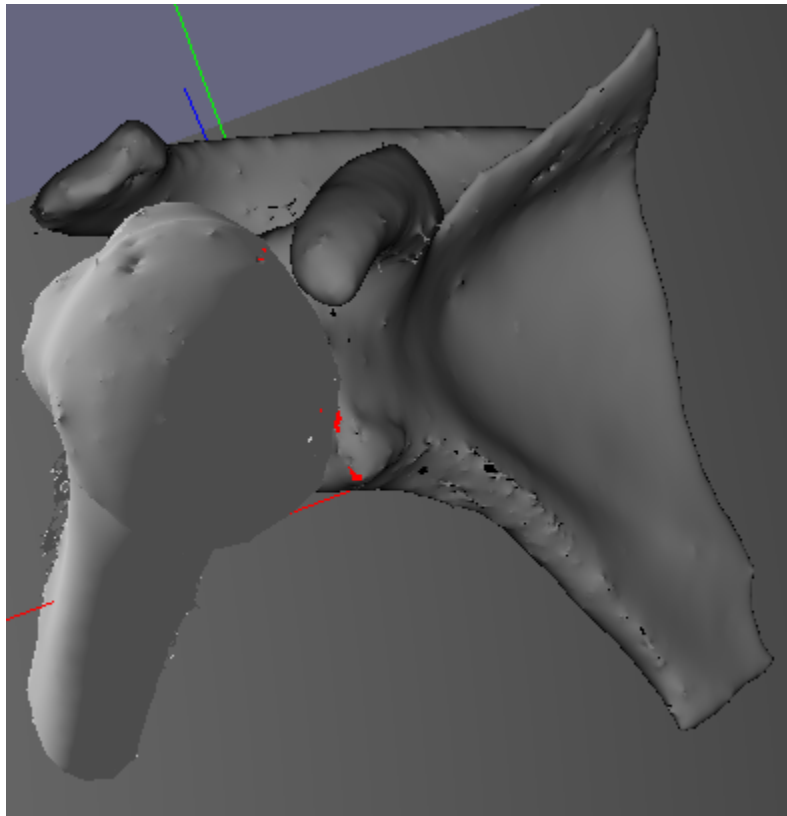


Figure 3.6: Front View of the Critical Position

There exists another solution where one of the lines' vertices are inverted compared to the other. We also calculate and display this solution.

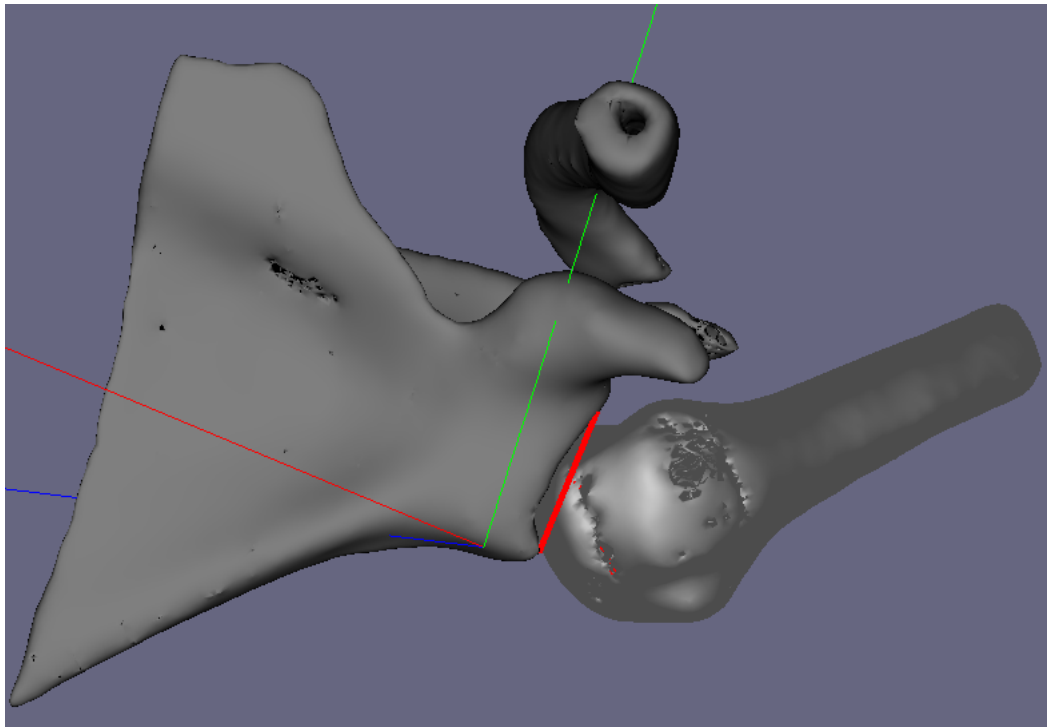


Figure 3.7: Another Possible Critical Position



# Chapter 4

## Software Pipeline

The concept of 3D visualization of DICOM data is not a new one, which is fortunate because it allows us access to open-source tools that expedite portions of our software concept that already have implementations. 2D DICOM visualizers, 3D reconstruction algorithms, mesh modification software and GUI libraries were surveyed according to their usefulness and formed into a software pipeline. In this chapter, we will illustrate the data flow and describe this pipeline.

### 4.1 Software Program Pipeline

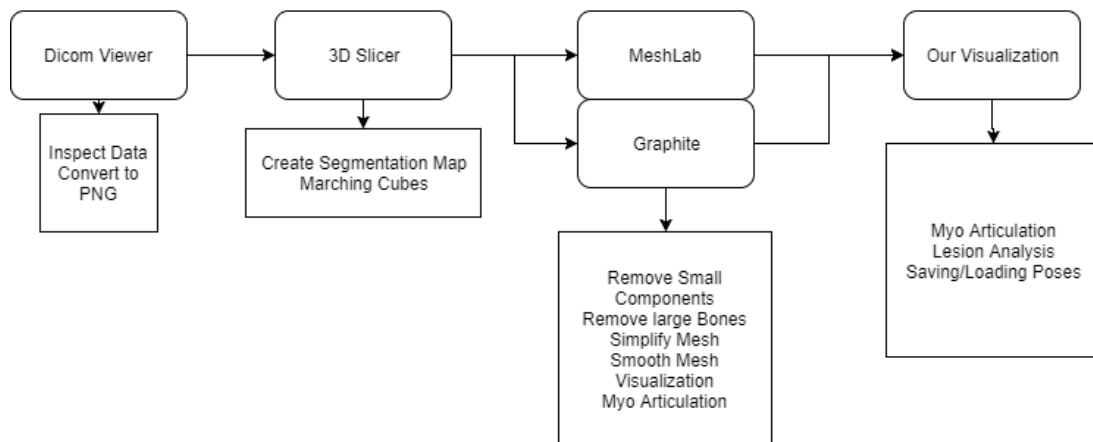


Figure 4.1: An illustration of requirement compliance.

The first stage of our pipeline aims to view and manipulate DICOM data stored in a series. we use Health Sant's DICOM viewer to display the CT data series used in our research. The viewer allows us to see the black and white image of each CT slice, as well as the metrics specific to the scan, most critically: mm between slices, the field of view, and imaging modality. The slices are viewed on a reel, with the ability to scroll back and forth to simulate a sense of depth. Parsing manually through the image data of the CT in this way is sometimes as far as a surgeon will go before using the information to plan the surgery.

In our case, we were provided with a set of HSL cases and the corresponding treatment options that were decided on by the surgeon. No Post-Op data was provided. We use the viewer to visually inspect that the data is not corrupt or garbled before proceeding with further visualization steps. It is common for surgeons to use 2D data stored in this format to get a better sense of the wound geometry or to directly diagnose patients. This is done by shifting through the images one-by-one until the slice number of the wound shows up. Surgeons will typically shift back and forth to simulate a 3D version of the area in their mind's eye.

## **4.2 3D Slicer**

3D data allows surgeons to visualize 3D information directly, instead of inferring it from 2D DICOM data. Inspection of the 3D dimensional data allows another channel of information for the surgeon to work with when planning surgeries. Algorithms for crafting meshes from serial 2D data have existed for a long time. Of these, the Marching Cubes algorithm has proved a reliable algorithm for intuitively representing data in a manner attractive for surgeon surgery planning. Toward this end, we queried different possible solutions. Visualisation Tool Kit is an industry-standard generally used in 3D visualization applications. We chose a piece of open-source software named 3D Slicer, which was coded to use the VTK library as its engine, as it provided a potent implementation of the marching cubes algorithm[6].

Their algorithm ensures that the image intensities are representative of a surface that lies within and inside the boundaries of the shape, allows for smoothing iterations that preserve boundary information while helping with staircase artifacts, minimizes the number of polygons (and thus

file size), captures sharp features (such as breaks) effectively, and provides information that allows smooth lighting on the bone. The output of the algorithm results in a 3D object. However, there remains some work to make it useful.

### 4.3 Graphite and Meshlab

A problem with some modeling software is that they hide parameters used in the calculations of mesh functions that we would like to use. For example, the smoothing algorithm used by 3D slicer doesn't allow for fine control over the number of smoothing iterations. To get around issues like these, we use a fork of Graphite 2.0 because the software allows for direct, low-level control of the mesh processing algorithms we are interested in. We also use Meshlab for algorithms that are more generic and don't require a fine degree of control over their parameters[3] [2].

We make use of small-component filtering, manual deletion of the rib cages and other bones that are captured on the periphery of the imaging area, as well as mesh simplification and Laplacian Smoothing. The degree of smoothing applied was chosen specifically to preserve the signature of the HSLs present in our data, and is not expected to change the final position of the characteristic points of the approximating lines.

First in this section of the pipeline is the small-component filtering. This algorithm explores the mesh by traversing and marking the graph as it goes along. Once all of a vertex's neighbors have been marked it is considered explored. Once all connected vertices have been recursively marked, a count can be established. For our denoising step, we found that any piece of mesh with a vertex count below 1000 was very likely to represent noise present from the CT imaging process. The result of setting this parameter is a clear view of all the large bones of interest.

After that step, there are several bones present in the view that obscure the result. We choose to use a component deletion tool to remove the mesh elements that represent any bone that is not part of the glenohumeral joint structure. The component deletion tool uses a similar graph traversal method that begins at a clicked vertex and retrieves the minimal connected structure. Following this, the related connections and vertices can be eliminated.

Following this, we simplify the mesh. 3D Slicer yields meshes with an extremely large number

of vertices. This is advantageous for capturing precise edges and boundaries from the original DICOM data but is impractical from file storage and processing standpoint. By applying a Delauney Triangulation method, we reduce the number of vertices present in the images by an order of magnitude while preserving the features of the mesh. With a modern graphics card, this step can safely be skipped. It was specifically a quality of life change for the local (old) research desktop.- The characteristics of this algorithm ensure that the boundary information that we are interested in is visually preserved and still useful for diagnostic purposes. The principal gain is in the rendering time further down the pipeline.

Finally, we smooth the result. The reasoning behind this is that the earlier small-component removal does not take care of noise that intersects our boundary of interest. The choice of the Laplacian Smoothing algorithm[18] evens out this noise and presents a clear view of the region of interest.

We run this algorithm for 10 iterations, with weight 1. The effect is cumulative and reduces the incidence of mesh “spikes” that protrude from the mesh. The final product is suitable for 3D visualization in a VTK-like environment.

## 4.4 OpenGL GUI and Interaction

Our software allows the display and manipulation of 3D meshes. On using the “load” command, the user is allowed to select and load separated meshes prepared from earlier in the pipeline. The format also allows for the input of default line approximations of Hill-Sachs and Bankart lesions. Once loaded, the user can reposition the camera by panning, zooming, or rotating about the origin point. This allows the user to viewpoints of interest in the scans. Some lesions are subtle, necessitating these functions.

Other functions that allow manipulation of the viewpoint include the toggling of the default axes, humerus, or the scapula. These let the user get a better view of either the Bankart or the HS lesion. It was found during the course of usage that the approximating lines were often obscured by the boundary of the meshes. To solve this, we allow the toggling of the transparency of the meshes. This presents a clear view of the approximating lines.

## Chapter 5

# Myo and Engagement Detection

In this chapter, we talk about our usage of the Myo tracking bracelet and its use in posing our 3D reconstructed clinical data. First, we explain a common diagnostics scenario involving patient discomfort. This provided the background to an interest in providing the user with control schemes that allow them to pose humeral bone to observe different problem points. We describe a touch-and-drag control scheme, followed by a motion-detecting bracelet driven approach. We then provide a breakdown of the technology, specs, and common uses of the Myo bracelet, which was our chosen motion detector.

We explain the calibration procedure involved in the transformation of the Myo's LCS into our scene LCS, as well as threading communication concerns with the main program. Finally, we provide an end-to-end demonstration of the Myo in action.

## **5.1 Clinical Manual Shoulder Diagnosis**

Because of the repetitive nature of the dislocations, and additional degradation of the bone loss that occurs in a re-dislocating patient, the geometry of the problem changes over time. The surgeon we consulted with described a “rounding out” of the lesion, where the wear and tear of the bones rubbing against each other causes additional bone loss during dislocation events through the continuous interaction of the joint. Indeed, this occurrence is also supported in the literature, where the more often a shoulder is dislocated and the more hours it spends dislocated, the more often larger bone loss that can affect surgical management is likely to occur [12]

Dr. Martineau related to us that this would then cause him to require additional probing of the patient. First, his patient is placed comfortably after having their shoulder reduced back into its socket. During this process, Dr. Martineau would ask questions while positioning the patient’s shoulder to get a sense of which positions were most problematic for the patient. This served the purpose of rudimentary screening for patients that don’t require surgery, as well as a way to inspect the joint for its extent of disfunction.

There are several problems inherent to this process. Chief among them is patient discomfort. Dr. Martineau described anecdotally the reaction of a patient whose arm was close to dislocation. There is an extremely uncomfortable reflex where the patient can detect the point of motion that results in impending dislocation. This causes a large amount of anxiety and can result in pain. The patients undergoing this type of session will often have imaging data on file in the form of CT scans. Ordinarily, these serve the function of visually confirming the severity of the bone loss. In static form, they are of limited usability for assessing the breadth of motion available to the patient.

## **5.2 Method for re-orienting and displaying the points of interest**

We adopted two control schemes to manipulate the mesh in our scene. We hold that these would allow a Clinician to orient and position their patient’s 3D data themselves, to allow them to detect problem positions that could result in a repeat dislocation event without overly inconveniencing the patient and causing discomfort.

We chose to use a Right Anterior Superior coordinate frame for our world coordinate system as

an intuitive and familiar coordinate system to perform the bulk of our work in.

### 5.2.1 Manipulating the Bone via Track Ball

Here, we animate the bone using a simple 2 point transform skeleton and a screen-based selection ball drag-and-drop approach

The trackball controls are as follows

- Record a start point when the user clicks on the screen
- Record an endpoint when the user has dragged the mouse some distance and released the button
- Map the start and end points as  $(x, y)$  onto a virtual ball using  $(x)^2 + (y)^2 + (z)^2 = r^2$  solving for  $z$ , where with  $r = \min(w, h)$  where  $w$  and  $h$  are the screen width and height.
- define  $\tilde{s} = (center - start)$ , with center as  $(0, 0, 0)$
- define  $\tilde{e} = (center - end)$
- Calculate  $axis = s \times e$  and take  $norm(axis)$  to obtain the axis of rotation.
- Calculate  $\theta = \arccos \frac{(s \cdot e)}{|s||e|}$  where  $\theta$  is the magnitude of the rotation
- Apply an arbitrary scale factor to  $\theta$ , tune for usability
- For coordinates outside the virtual sphere, instead use  $axis = \tilde{k}$

This would hypothetically allow Dr. Martineau to move the virtual bone around intuitively as if he were rotating the shoulder in place by applying torque. This mirrors his previously described manipulation of his patient's shoulder. By supplementing patient examination with virtual examination, the simulation can be used to validate the Dr's thoughts.



### 5.3 Myo Specs



Figure 5.1: The Myo Armband [37]

LEDs	Dual Indicator LEDs			
Processor	ARM Cortex M4 Processor			
Vibrational Haptic Feedback	Short period	Medium period	Long period	
Sensors	9-axis IMU	3-axis magnetometer & accelerometer	3-axis containment gyroscope	Medical Grade Stainless Steel EMG sensors

Table 5.1: Myo Specs

In conjunction with this setup, we propose the usage of the Myo Armband to provide the transformation matrices representing the movement of the arm. The Myo Armband uses a 3 axis gyroscope, accelerometer, and magnetometer. The device is flexible and can be placed around the bicep of the individual that wants to articulate the data. When calibrated, this would allow the user to position their arm and see the corresponding action play out on their computer screen.

To recuperate and use the transform generated by the Myo, it's important to know how it is calculated. This is because we must generate a coordinate frame transform to transfer the relative movements of the bracelet satisfactorily to the frame inside the application.

One of the vectors is relative to the magnetic influence of the earth and a second vector points out from the blue LED logo when it was first turned on.

The LCS can be either a left-handed or right-handed coordinate frame, depending on the particular convergence of the algorithm when the Myo boots up.

## 5.4 Manipulating the Bone via Myo

We add a two-point animation skeleton to the cleaned 3D data, to provide a local coordinate frame for applying the Myo bracelet's transform. A center of rotation in the middle is manually placed such that it roughly coincides with the centroid of the humeral head. This provides a basis for movements that is intuitive to a user of the motion detection bracelet.

At the outset of a trial, the coordinate system of the user and the coordinate system of the camera scene are not in sync. To make it so that the bone behaves predictably in our scene, such as raising to the right as the user raises their right arm, we must calculate the fixed offset between the two coordinate systems.

To retrieve this offset, we created a simple two-step procedure.

- We affix the handedness of the system internally because the Myo bracelet will choose either a right or left-handed system when started up
- We fix the downward position of the Myo to determine our coordinate system's "Up" direction.
- We map the partial offset to our scene and begin to allow the bone to move according to the rotation emitted by the Myo
- We have the user raise their hand forward. This will result in the bone on the screen rotating in the transverse plane. This is often the wrong rotation
- We correct for this by adding a transverse plane offset a degree at a time as a key is held down. The calibration is complete when the arm's direction visually matches the scene humerus' direction



Figure 5.2: Initial Myo Position



Figure 5.3: First calibration position



Figure 5.4: Second calibration position

## Chapter 6

# Conclusion and Further Avenues of Research

### 6.1 Conclusion

We examined Hill-Sachs Lesions, wedge-shaped humeral head injury to the shoulder that can cause a repeated shoulder dislocation.

Researching the HSL was an interesting dive into a growing sector of cooperative research between the fields of 3D imaging and Orthopedics. Through this research, we had many conversations with the target users of our tool that provided a different angle of focus on the utility of positioning and collision in virtual environments.

In this work, we determined that there was a dearth of visualization tools for diagnosing HSL from the perspective of the surgeon, which motivated us to settle the matter of whether a 3D visualization of a patient's CT or MRI scans could be used for HSL diagnosis and/or planning of reduction surgery. We demonstrated a software pipeline that transforms a set of DICOM images into a 3D scene where they can be manipulated to allow a surgeon to better plan their surgeries.

We demonstrated the design of a new HSL diagnostic heuristic. To provide a setting, we explained the historical clinical concepts of percent volume bone loss and the Glenohumeral Track and why they sometimes prove ineffective as diagnostic heuristics for assessing the chance of re-impingement. We explained the logic behind a simplified translation/rotation measure formulation

for determining possible problem-positions for shoulder impingement, and how these could be applied via a feature selection scheme.

We were also interested in posing methods and calculations that could serve as a stand-in for stressful patient physical examinations. We showed a calculation for automatically computing possible problem positions and outlined a click-and-drag control scheme, as well as a calibrated control scheme involving the Myo bracelet to pose our clinical data. We provided an argument for why these would be good candidates for supplementing Dr. Martineau's manual manipulation of an injured patient's arm; they can manipulate 3D data in addition.

## **6.2 Limitations and Future Work**

Our hope with this research is that it can be expanded in the future to encompass a planning software that could be used to help treat patients that suffer from this unfortunate and painful injury.

### **6.2.1 Surgeon Survey**

An important test for one of our main contributions, the line and measure characterization of the HSL, would be a clinical study conducted using the tool. While developing, we discussed having a study put together to contrast two control groups of surgeons that would test the discriminatory ability of our measures. The study design would compare a group using traditional scans vs. a group using the 3D tool. An interesting variable to track long-term would be the quality of patient recovery. Regrettably, this study could not be performed because of both organizational and technical limitations.

There are several limitations concerning the demo availability of this program. The location of the point of articulation at the center of the humerus is a limitation in the work. The points as shown in the tool are manually placed and saved between runs, using a trial and error process. We initially worked in the 2D domain attempting to fit circles to the DICOM images and there exist some least-squares spherical regression techniques that can locate this center, but they were similarly not pursued because of scope constraints. Such a feature would be a marked quality of life improvement when using the tool.

Having a save feature that maintains positions of interest between runs is also somewhat limited to a very manual process that can only tolerate one saved position.

The program is statically linked with libraries that the user must find and include to run it. This posed no issues for our testing of the concepts of the program but is relevant when trying to circulate the program to prospective study participants and/or demo machines. More attention would need to be placed on the build system of the software to realize the technical side of things.

Many solutions visualize and allow planning, but to our knowledge, there are no visualization platforms that feature the couple of techniques that were developed for manipulating the HSL feature areas of the mesh specifically.

### **6.2.2 MRI vs CT**

MRI imaging is an interesting venue for this sort of research. In our experience using MRIs, there was too much noise around bones and too few slices to provide a diagnostically interesting surface to work from. In the first case, choosing among higher powered and more modern MRI machines and choosing different imaging parameters could both mitigate the noise problem that we observed and the bone could presumably be picked out more easily.

This would require closer collaboration from the hospital and a selection of patients. The large staircase artifacts are a bigger problem. Slice thicknesses in CT images were in the 0.1mm range and provide a nice boundary. However, MRI imaging tends to degrade at slice thicknesses below 1mm.

This decreases the effectiveness of a standard segmenting/marching cubes approach. Different approaches that either interpolate data more flexibly than marching cubes (spline interpolation) or CNN based fitting/denoising algorithms run on smaller thicknesses could mitigate this issue and present a useful model from a source of data that incurs no radiation dose on the patient's part.

## **6.3 Graph Cuts**

Graph cuts are an alternative segmentation method to the simple thresholding used in our pipeline. It's an algorithm that takes a global view of the image cells and attempts to minimize an objective

energy function.

The energy function typically uses pixel intensity and coherence parameters along with some constraints to represent a maximum "flow" and a minimum "cut" between background and foreground pixel segments. The objective function produces a segmentation when the "flow" values of labeled pixels between two chosen seed points are maximized.

A sample function could be implemented as follows:

$$E(L) = \sum_{p \in P} D_p(L_p) + \sum_{(p,q) \in N} V_{p,q}(L_p, L_q) [10]$$

L is a labeling of the image, D penalizes using intensities and a likelihood function, V is a spatial coherence penalty for discontinuities, P is the examined pixel, N is neighboring pixels.

In this thesis, a simpler thresholding technique was used. When more generous thresholds were applied, this would cause large connected components to appear on the surface of the bone. Because of this, more conservative thresholds were selected that possibly underestimated the true boundary of the mesh. Substituting this stage of the pipeline with graph cuts would potentially allow us not to worry about removing small components, re-meshing, nor applying a Laplacian operator as aggressively.

Staircase artifacts would be preserved and would be tackled using a more conservatively calibrated Laplacian or other interpolation technique.

### 6.3.1 Finite Element Analysis

Finite Element Analysis is a physical simulation method where a complicated process in a continuous domain is divided into simpler finite elements that are easier to calculate. The individual elements are typically a representative set of partial differential equations that model some physical process of interest. The humeral head and glenohumeral joint are ideal inputs, as they are already divided into the necessary discrete elements.

There exist similar examples in the literature that have simulated joint physics for shoulders to evaluate shoulder implant performance [9] or to evaluate the realism of the glenoid track concept[34].

We posit that if the boundary of the two lesions can be retrieved, a similar technique could be applied to figure out when the two lesions collide and stick. An iterative model where the objects

are perturbed by simulated shoulder muscle could be combined with a friction and/or stress force analysis to more accurately gauge the final problem orientations for the patient's data.

### **6.3.2 Myo Error**

For using the Myo bracelet to control the mesh, our results were visually appealing, in that we attained corresponding movements between the on-screen bone and the user's humerus. However, this method of control has some important limitations. There are some issues in the construction of the bracelet, namely that the piece that deforms is plastic. This means that over time, there can be unsteady errors introduced.

Also, prospective users necessarily have different anatomy from whichever patient is being modeled. This could mean that there are important biomechanical adjustments to be characterized and adjusted for when moving someone else's bone scans around. The bounding and correction of this anatomical error remain an open research question.



# Appendix A

## Bibliography

- [1] Frederic srouer - <https://www.facebook.com/epaulet.o.p/posts/2410278782550296/>.
- [2] Graphite <http://alice.loria.fr/software/graphite/doc/html/>.
- [3] Meshlab - <http://www.meshlab.net/>. Accessed: 2020-01-19.
- [4] 3d slicer marching cubes result - <https://blog.kitware.com/3d-slicer-4-10-1-improves-segmentation-effects-and-adds-video-management-infrastructure/>, Jan 2019.
- [5] PATRICK J. DENARD, STEPHEN S. BURKHART. Diagram demonstrating a latarjet procedure - <https://musculoskeletalkey.com/latarjet-procedure-for-instability-with-bone-loss-2/>. Accessed: 2020-01-18.
- [6] 3DSLICER COMMUNITY. Model maker feature from 3d slicer - <https://www.slicer.org/wiki/modules:grayscalemodelmaker-documentation-3.6>, 2019. Accessed: 2019-07-18.
- [7] ARCIERO, PARRINO, E. A. The effect of a combined glenoid and hill-sachs defect on glenohumeral stability. *The American Journal of Sports Medicine* 43, 9 (Mar. 2015).
- [8] AUFFARTH, A., MAYER, M., KOFLER, B., HITZL, W., BOGNER, R., MORODER, P., KORN, G., KOLLER, H., AND RESCH, H. The interobserver reliability in diagnosing osseous

- lesions after first-time anterior shoulder dislocation comparing plain radiographs with computed tomography scans. *Journal of Shoulder and Elbow Surgery* 22, 11 (2013), 1507-1513.
- [9] BCHLER, P., AND FARRON, A. Benefits of an anatomical reconstruction of the humeral head during shoulder arthroplasty: a finite element analysis. *Clinical Biomechanics* 19, 1 (2004), 1623.
- [10] BOYKOV Y., K. V. An experimental comparison of min-cut/max- flow algorithms for energy minimization in vision. *IEEE Transactions on Pattern Analysis and Machine Intelligence* 26, 9 (2004), 1124-1137.
- [11] BRODY, W. R., BUTT, G., HALL, A., AND MACOVSKI, A. A method for selective tissue and bone visualization using dual energy scanned projection radiography. *Medical Physics* 8, 3 (1981), 353-357.
- [12] BURKHART, S., DAI, X., AND DENARD, P. Increasing preoperative dislocations and total time of dislocation affect surgical management of anterior shoulder instability. *International Journal of Shoulder Surgery* 9, 1 (2015), 1.
- [13] CALANDRA, BAKER, U. The incidence of hill-sachs lesions in initial anterior shoulder dislocations. *The Journal of Arthroscopic and Related Surgery* 5, 1 (Dec. 1989), 254–257.
- [14] CHO SH, CHO NS, R. Y. Preoperative analysis of the hill-sachs lesion in anterior shoulder instability: how to predict engagement of the lesion. *The American Journal of Sports Medicine* 39, 6 (Nov. 2011), 2389–2395.
- [15] DEAN, C. J., SYKES, J. R., COOPER, R. A., HATFIELD, P., CAREY, B., SWIFT, S., BACON, S. E., THWAITES, D., SEBAG-MONTEFIORE, D., MORGAN, A. M., AND ET AL. An evaluation of four ct-mri co-registration techniques for radiotherapy treatment planning of prone rectal cancer patients, Jan 2012.
- [16] DI GIACOMO, G., ITOI, E., AND BURKHART, S. S. Evolving concept of bipolar bone loss and the hill-sachs lesion: From “engaging/non-engaging lesion to “on-track/off-track lesion. *Arthroscopy: The Journal of Arthroscopic & Related Surgery* 30, 7 (Oct. 2013), 90–98.

- [17] DR MAULIK S PATEL. X-ray of a hill sachs lesion - <https://radiopaedia.org/cases/hill-sachs-lesion-4?lang=us>. Accessed: 2020-01-18.
- [18] FIELD, D. A. Laplacian smoothing and delaunay triangulations. *Communications in Applied Numerical Methods* 4, 6 (1988), 709712.
- [19] G., B. B. Winged edge polyhedron representation. *STANFORD UNIV CA DEPT OF COMPUTER SCIENCE* 2, 8 (1972).
- [20] GARCIA, G., TAYLOR, S., FABRICANT, P., AND DINES, J. Shoulder instability management: A survey of the american shoulder and elbow surgeons. *American Journal of Orthopedics* (2016), E91–E97.
- [21] GYFTOPOULOS, S., YEMIN, A., AND BENCARDINO, J. Engaging hill-sachs lesion: Is there an association between this lesion and findings on mri? *American Journal of Roentgenology* 201, 4 (2013).
- [22] HALAI, M., HESTER, T., AND BUCKLEY, R. E. Does 3d ct reconstruction help the surgeon to preoperatively assess calcaneal fractures? *The Foot* 43 (2020), 101659.
- [23] HAMILTON, W. R. Xxxix. on quaternions; or on a new system of imaginaries in algebra. *The London, Edinburgh, and Dublin Philosophical Magazine and Journal of Science* 25, 166 (1844), 241246.
- [24] HELLERHOFF. Illustration of engaging hill sachs lesion - <https://en.wikipedia.org/wiki/hill> Accessed: 2020-01-18.
- [25] HERMAN, G. T. Three-dimensional imaging on a ct or mr scanner. *Journal of Computer Assisted Tomography* 12, 3 (1988).
- [26] HILL, H. A., AND SACHS, M. D. The grooved defect of the humeral head. *Radiology* 35, 6 (1940), 690700.
- [27] KACZMARZ, S. Approximate solution of systems of linear equations. *International Journal of Control* 57, 6 (1993), 12691271.

- [28] KUHL, D. E., AND EDWARDS, R. Q. Image separation radioisotope scanning. *Radiology* 80, 4 (1963), 653662.
- [29] LEE, J. K., YAO, L., PHELPS, C. T., WIRTH, C. R., CZAJKA, J., AND LOZMAN, J. Anterior cruciate ligament tears: Mr imaging compared with arthroscopy and clinical tests. *Radiology* 166, 3 (1988), 861864.
- [30] LORENSEN, W. E., AND CLINE, H. E. Marching cubes: A high resolution 3d surface construction algorithm. *Proceedings of the 14th annual conference on Computer graphics and interactive techniques - SIGGRAPH 87* (1987).
- [31] MAGNE, P. Efficient 3d finite element analysis of dental restorative procedures using micro-ct data. *Dental Materials* 23, 5 (2007), 539548.
- [32] OHIO STATE UNIVERSITY MEDICAL CENTER. Illustration of horizontal extension of the arm in a human male - <https://www.yumpu.com/en/document/read/4183078/scapular-shoulder-and-elbow-theraband-the-accidental-amazon/7>, Sep 2009. Accessed: 2020-01-18.
- [33] OLDENDORF, W. H. The quest for an image of brain: A brief historical and technical review of brain imaging techniques. *Neurology* 28, 6 (Jan 1978), 517517.
- [34] PCORA, JOS OTVIO REGGI, E. A. glenoid track evaluation by a validated finite-element shoulder numerical model. *Orthopaedics and Traumatology: Surgery and Research* 2, 8 (2020).
- [35] PHAM N., MORRISON A., S. J. A.-R. S. I. V. . T. M. E. A. Quantitative image analysis of immunohistochemical stains using a cmyk color model. *Diagnostic Pathology* 2, 8 (2007).
- [36] RADON, J. On the determination of functions from their integral values along certain manifolds. *IEEE Transactions on Medical Imaging* 5, 4 (1986), 170176.
- [37] ROBYN. Picture of a myo bracelet - <https://macsources.com/myo-armband-available-on-amazon/>. Accessed: 2020-01-18.
- [38] RSATUSZ. Scan showing a bony bankart lesion - [https://commons.wikimedia.org/wiki/file:cr\\_bony\\_bankart\\_lesion\\_with\\_stationary\\_fragment\\_at\\_the\\_inferior\\_gle](https://commons.wikimedia.org/wiki/file:cr_bony_bankart_lesion_with_stationary_fragment_at_the_inferior_gle). Accessed: 2020-01-18.

- [39] SAITO, H., ITOI, E., MINAGAWA, H., YAMAMOTO, N., TUOHETI, Y., AND SEKI, N. Location of the hill-sachs lesion in shoulders with recurrent anterior dislocation. *Archives of Orthopaedic and Trauma Surgery* 129, 10 (2009), 13271334.
- [40] SITTING, D. F., ASH, J. S., AND LEDLEY, R. S. The story behind the development of the first whole-body computerized tomography scanner as told by robert s. ledley. *Journal of the American Medical Informatics Association* 13, 5 (Jan 2006), 465469.
- [41] SRIVATSAN, R. A., ROSEN, G. T., MOHAMED, D. F. N., AND CHOSET, H. Estimating se(3) elements using a dual quaternion based linear kalman filter. *Robotics: Science and Systems XII* (2016).
- [42] STREUBEL, P. N., KRYCH, A. J., SIMONE, J. P., DAHM, D. L., SPERLING, J. W., STEINMANN, S. P., ODRISCOLL, S. W., AND SANCHEZ-SOTELO, J. Anterior glenohumeral instability. *Journal of the American Academy of Orthopaedic Surgeons* 22, 5 (2014), 283294.
- [43] SUN YAO. Illustration of local coordinate systems common to the medical field - [https://blog.csdn.net/sunyao\\_123/article/details/72801429](https://blog.csdn.net/sunyao_123/article/details/72801429). Accessed: 2020-01-18.
- [44] THIEL, G. S. V., GHODADRA, N. S., ROMEO, A. A., AND PROVENCHER, M. T. Management of chronic shoulder dislocations. *Shoulder Instability: A Comprehensive Approach* (2012), 487504.
- [45] THINK SURGICAL, I. Tsolution one tha stem application animation - [https://www.youtube.com/watch?time\\_continue=30&v=ek0\\_c2\\_z2mu](https://www.youtube.com/watch?time_continue=30&v=ek0_c2_z2mu), Jan 2018.
- [46] UNKNOWN. Diagram demonstrating a remplissage procedure - <https://www.shoulderdoc.co.uk/article/1300>. Accessed: 2020-01-18.
- [47] UNKNOWN. Hill-sachs lesion - <https://centralcoastortho.com/patient-education/hill-sachs-lesion/>, Jul 2017. Accessed: 2019-07-19.
- [48] UNKNOWN. Illustration of external rotation of the arm in a human male - <https://www.reddit.com/r/bodyweightfitness/comments/aip3fj/>, 2019. Accessed: 2020-01-18.

- [49] YAMAMOTO, N., ITOI, E., ABE, H., MINAGAWA, H., SEKI, N., SHIMADA, Y., AND OKADA, K. Contact between the glenoid and the humeral head in abduction, external rotation, and horizontal extension: A new concept of glenoid track. *Journal of Shoulder and Elbow Surgery* 16, 5 (2007), 649-656.

## Appendix A

# Appendix A - Code

The following scheme and increments were used to adjust the second calibration vector:

```
LCScorrection = QQuaternion::fromAxisAndAngle(QVector3D(1.0, 0.0, 0.0), 90.0);

float pitch;
float yaw;
float roll;
//humerusRotation is a variable that tracks the current mapping
between the humerus and the Myo.
humerusRotation.getEulerAngles(&pitch,&yaw,&roll);
LCScorrection2 = QQuaternion::fromAxisAndAngle(QVector3D(0.0,1.0,0.0),
-(yaw+180.0));
if (e->key() == Qt::Key_D)
{
LCScorrection2 = QQuaternion::fromAxisAndAngle(QVector3D(0.0,1.0,0.0),
calibAngle);
calibAngle += 1.0;
} else if (e->key() == Qt::Key_A)
{
LCScorrection2 = QQuaternion::fromAxisAndAngle(QVector3D(0.0, 1.0,0.0),
calibAngle);
calibAngle -= 1.0;
}
```

Once the LCS is calibrated, it is applied to every point on the mesh that we load as follows:

```
QVector3D ObjModel::getRotatedVertex(QVector3D vertex, QQuaternion quatToApply,
    QVector3D rotationalCenter)
{
    QQuaternion translationRemoved = QQuaternion(1.0,
    vertex.x()-rotationalCenter.x(),
    vertex.y() - rotationalCenter.y(),
    vertex.z() - rotationalCenter.z());

    QQuaternion rotatedPoint = quatToApply * translationRemoved * quatToApply.
        conjugate();

    QQuaternion rotatedAndTranslatedPoint = QVector3D(rotatedPoint.x() +
        rotationalCenter.x(),
    rotatedPoint.y() + rotationalCenter.y(),
    rotatedPoint.z() + rotationalCenter.z());

    return rotatedAndTranslatedPoint;
}
```

The translational component is removed before applying the quaternion. This is because, unlike transformation matrices, quaternions do not preserve transformation order other than rotation. This way, the point may still be successfully rotated.



## **Appendix B**

# **Appendix A - Vicon Experiment**

Since we are using the Myo to articulate the patient's humeral bone mesh through the proxy of the wearer's bicep, we acknowledge some error between the orientation provided by the Myo and the actual joint mechanics of the patient's real arm. We are curious to quantify different dimensions of this error.

What is the true rotational error between the Myo bracelet and the rotation about the pivot point located at the center of the patient's humerus? Is the calibration procedure we have outlined in this thesis repeatable?

The Vicon is a 3D calibrated 6 camera system that uses active tracking to localize points in 3D space with a degree of accuracy sufficient enough for tracking actors in full-body active-tracking bodysuits while they perform various physical feats that are translated into 3D animation contexts. We hypothesize that the Vicon is more accurate than the Myo, and can be used as ground truth for measuring against the Myo's orientation as an actor moves it through some simple paused arm motions that a surgeon may attempt while articulating the patient's data.

### **B.1 Experiment Outline**

- place myo on ground, turn on
- record a myo calibration frame

- place myo on actor’s right bicep
- position actor on central Vicon platform
- attach 4 active markers with tape to the actor’s arm
- begin continuous recording on Myo
- assume a static position and record Vicon snapshot
- repeat until the end of the motion

This experiment was repeated 6 times to generate 6 blocks of data.

## B.2 Data Post-Processing

The Myo outputs data in a quaternion format. These quaternions were recorded for the duration of each block and written to a text file.

The Vicon data is saved as 4 points per frame saved.

The first change was to convert the Vicon data from points into orientation changes between the frames.

We computed a covariance matrix and solved the resulting constraints that were produced by using the Singular Value Decomposition method.

This yielded

Block	1	2	3	4	5	6
Myo Frames	252	315	210	231	168	273
Vicon Frames	11	12	7	7	7	11

Table B.1: Frames

There is a large sampling difference between the Myo and Vicon frames. To correct this problem we chose to downsample the Myo based on a threshold. This was where the experimental design played its part. Frames that we saved could be distinguished by others because they were followed by a rapid movement that causes a large change in rotation angle between any two given matrices.

We defined that any movement over 2 degrees would denote a transition between actor poses, and chose the frame immediately before this change as our downsampling strategy. This yielded

Block	1	2	3	4	5	6
Downsampled Myo Frames	11	16	10	11	8	13
Vicon Frames	11	12	7	7	7	11

Table B.2: Frames Downsampled

Now that the correspondence problem had been sufficiently reduced, we began to search for a proper local coordinate system(LCS) transform to map between the two coordinate spaces.

The calibration matrix collected from the experiment could not be used, as we discovered on inspection of the data that the coordinate frame shifted between blocks, which suggests that the Myo may sometimes reset its internal coordinate frame calculation depending on its programming.

Instead, we created a large number of possible LCS transformations with fixed up vectors and iteratively searched them for the one that best fits the majority of the corresponding frames.

The frames were compared with the dot product between them.

$$\theta = \frac{(M^t \cdot V)}{|M^t||V|}$$

An alignment index offset for the block was chosen, since the Myo blocks still have more frames than the Vicon blocks. These were found by inspection. In block 2, for example, frames 2-14 of the Myo were compared with frames 0-12 of the Vicon.

The chosen LCS minimized the total degree error of a block, given a particular alignment.

### **B.3 Discussion and Limitations**

As can be seen from the data, the Myo can track the Vicon to within 45 degrees or so, but multiple sources of error cause the correspondence problem between their coordinate systems to be difficult to solve.

Outliers are generated because of dead frames in the Vicon, the Myo will occasionally register a large degree of orientation change during sudden motions and the Myo will sometimes reset its coordinate reference frame while running.

These outliers cause the fit to be constrained to suboptimal LCS registrations between the data sets. It is possible that a more robust protocol that verifies correspondences could yield a better fit than is illustrated here. Notable difficulties were the downsampling due to obfuscated points and the synchronization between the Myo and the Vicon.

As a result of these issues, further inquiry is warranted. It is notable that there seems to be no pattern of drift in the data, and that the outliers effect dominates.

## B.4 Data

$$Block1LCS = \begin{pmatrix} 0.42910195 & -0.90274444 & -0.03039737 \\ -0.85614438 & -0.39576406 & -0.3322463 \\ 0.28790332 & 0.16859207 & -0.9427027 \end{pmatrix}$$

Myo Frame	Vicon Frame	Degree Difference
1	1	61.40711438341727
2	2	37.90295661615284
3	3	21.10860233249938
4	4	49.490507315482446
5	5	11.321764761794268
6	6	36.16127019520871
7	7	12.286616072517639
8	8	25.934781476719447
9	9	12.63402600910483
10	10	42.44483714910317
11	11	62.648200665640026
Total Error	373.34067697764004	

Table B.3: Block 1

$$Block2LCS = \begin{pmatrix} -0.36710919 & -0.92526148 & 0.09550936 \\ 0.73245641 & -0.35083805 & -0.58345545 \\ 0.57335717 & -0.14423542 & 0.80650957 \end{pmatrix}$$

Myo Frame	Vicon Frame	Degree Difference
3	1	67.9009513164306
4	2	7.932168400611021
5	3	7.0733284695301375
6	4	24.10784145634804
7	5	31.8972384967495
8	6	25.85101211159616
9	7	27.329887738249646
10	8	34.31244595713465
11	9	11.280221543927423
12	10	21.87116292806589
13	11	26.79809262803376
14	12	61.440339305270586
Total Error	347.7946903519474	

Table B.4: Block 2

$$Block3LCS = \begin{pmatrix} -0.95214402 & 0.14449169 & -0.26933978 \\ 0.17028055 & -0.48102344 & -0.8600122 \\ -0.25382336 & -0.8647188 & 0.43339947 \end{pmatrix}$$

Myo Frame	Vicon Frame	Degree Difference
2	1	53.99900793127042
3	2	30.554428254793038
4	3	1.3192065489821634
5	4	15.451544772595781
6	5	30.63915449716881
7	6	32.92339127232038
8	7	24.549053772918214
Total Error	189.43578705004882	

Table B.5: Block 3

$$Block4LCS = \begin{pmatrix} -0.98053089 & -0.00111408 & -0.19636176 \\ 0.17535723 & -0.45498344 & -0.87306352 \\ -0.08836869 & -0.8904992 & 0.44632068 \end{pmatrix}$$

Myo Frame	Vicon Frame	Degree Difference
2	1	141.58526081298817
3	2	46.72218094769663
4	3	26.561466710214322
5	4	32.44906366088813
6	5	20.460409805436765
7	6	24.861770012639134
8	7	27.54128475130746
Total Error	373.34067697764004	

Table B.6: Block 4



$$Block5LCS = \begin{pmatrix} -0.41452907 & -0.85008794 & -0.32483249 \\ 0.82706858 & -0.50082434 & 0.25521078 \\ -0.37963563 & -0.16286646 & 0.91068727 \end{pmatrix}$$

Myo Frame	Vicon Frame	Degree Difference
1	1	81.1266494500507
2	2	66.77759396394407
3	3	28.95671181731437
4	4	37.51306398660618
5	5	8.128968199646332
6	6	80.99576054389236
7	7	78.14219582023158
Total Error		381.64094378168556

Table B.7: Block 5

$$Block6LCS = \begin{pmatrix} -0.97683712 & 0.02986703 & -0.21188958 \\ 0.17469664 & -0.46052407 & -0.87028654 \\ -0.12357312 & -0.8871446 & 0.44463934 \end{pmatrix}$$

Myo Frame	Vicon Frame	Degree Difference
2	1	46.009790368230554
3	2	33.70719853836567
4	3	37.89976675564392
5	4	59.97538372322299
6	5	71.17392539597878
7	6	94.34247773074237
8	7	61.49776308712457
9	8	79.93617020254166
10	9	22.33644765297646
11	10	15.328183082819839
12	11	36.7456433058131
Total Error	558.95274984346	

Table B.8: Block 6